

Factorization and Shape-Function Effects in Inclusive B-Meson Decays

S. W. BOSCH, B. O. LANGE, M. NEUBERT, AND G. PAZ

*Institute for High-Energy Phenomenology
Newman Laboratory for Elementary-Particle Physics, Cornell University
Ithaca, NY 14853, U.S.A.*

Abstract

Using methods of effective field theory, factorized expressions for arbitrary $\bar{B} \rightarrow X_u l^- \bar{\nu}$ decay distributions in the shape-function region of large hadronic energy and moderate hadronic invariant mass are derived. Large logarithms are resummed at next-to-leading order in renormalization-group improved perturbation theory. The operator product expansion is employed to relate moments of the renormalized shape function with HQET parameters such as m_b , $\bar{\Lambda}$ and λ_1 defined in a new physical subtraction scheme. An analytic expression for the asymptotic behavior of the shape function is obtained, which reveals that it is not positive definite. Explicit expressions are presented for the charged-lepton energy spectrum, the hadronic invariant mass distribution, and the spectrum in the hadronic light-cone momentum $P_+ = E_H - |\vec{P}_H|$. A new method for a precision measurement of $|V_{ub}|$ is proposed, which combines good theoretical control with high efficiency and a powerful discrimination against charm background.

1 Introduction

Inclusive B -meson decays into light final-state particles, such as the semileptonic process $\bar{B} \rightarrow X_u l^- \bar{\nu}$ and the radiative process $\bar{B} \rightarrow X_s \gamma$, are of great importance to the determination of the Cabbibo–Kobayashi–Maskawa (CKM) matrix element $|V_{ub}|$ and play a prominent role in the search for New Physics at the B factories. The ever increasing accuracy of experimental data on the inclusive decay rates and spectra provides a strong incentive to continuously improving the theoretical description of these processes. To keep up with the reduction of experimental errors, it will soon be necessary to have theoretical predictions for inclusive decay distributions with uncertainties below the 10% level.

There are several challenges facing theorists pursuing this ambitious goal. Due to experimental cuts one is generally faced with a situation where the hadronic final states are constrained to have large energy $E_H \sim M_B$ but only moderate invariant mass $s_H \sim M_B \Lambda_{\text{QCD}}$. In this kinematic region (called the “shape-function region”), the decay rates and spectra are obtained using a twist expansion [1, 2, 3], which is considerably more complicated than the conventional heavy-quark expansion employed in the calculation of inclusive rates for $\bar{B} \rightarrow X_c l^- \bar{\nu}$ decays [4, 5, 6]. In the twist expansion, infinite sets of power corrections are resummed into non-perturbative “shape functions” describing the internal structure of the B meson. At the same time, the short-distance corrections are also more complicated than in most other applications of heavy-quark expansions, because the kinematics implies the relevance of three separated mass scales: M_B (“hard”), $\sqrt{M_B \Lambda_{\text{QCD}}}$ (“hard-collinear”), and Λ_{QCD} (“soft”). Large logarithms of ratios of these scales arise at every order in perturbation theory and must be resummed [7, 8, 9]. To properly disentangle the physics associated with these scales requires a sophisticated effective field-theory machinery [10], which has only been fully developed recently. A systematic treatment consists of matching QCD onto soft-collinear effective theory (SCET) in a first step, in which hard quantum fluctuations are integrated out. In a second step, SCET is matched onto heavy-quark effective theory (HQET), and hard-collinear modes are integrated out. The resulting expressions for inclusive differential decay rates have the factorized form $d\Gamma \sim H J \otimes S$ [8, 9]. The function H contains the hard corrections, the jet function J , which describes the properties of the final-state hadronic jet, contains the hard-collinear effects, and the shape function S accounts for the internal soft dynamics in the B meson [1, 2]. The \otimes symbol implies a convolution over a light-cone momentum variable ω associated with the residual momentum of the b quark inside the B meson.

Up until now, no complete next-to-leading order predictions for inclusive decay rates and spectra in the shape-function region have been presented in the literature. In the present paper we close this gap. We go beyond previous work in several important ways. First, we complete the matching calculations for the two-step matching $\text{QCD} \rightarrow \text{SCET} \rightarrow \text{HQET}$ at next-to-leading order in perturbation theory. We then derive renormalization-group equations governing the dependence of the functions H , J , and S on the renormalization scale, and solve these equations analytically in momentum space. Next, we derive several model-independent properties of the shape function S , which were so far unknown. In particular, we present the precise form of the relations between renormalized shape-function moments and HQET parameters such as $\bar{\Lambda}$ and λ_1 , and we give an analytical formula for the asymptotic behavior of the shape function. An unexpected outcome of this analysis is the finding that the shape

function is not positive definite, but acquires a negative radiative tail at large values of $|\omega|$. We also discuss how to derive shape-function independent relations between different decay spectra, which are free of spurious Landau-pole singularities. This improves on similar relations that can be found in the literature [11, 12, 13]. Finally, we propose a new method for a high-precision determination of $|V_{ub}|$, which offers several advantages over previous approaches for extracting this important CKM parameter.

The remainder of this paper is organized as follows: In Section 2, we present a derivation of the factorization formula for inclusive rates in the shape-function region using the position-space formulation of SCET. The one-loop matching calculations needed to derive perturbative expressions for the functions H , J , and S are presented in Section 3. In Section 4, we derive evolution equations for these functions and present their exact analytic solutions in momentum space. A comprehensive discussion of the properties of the shape function is given in Section 5. While much of the discussion in this paper is necessarily rather technical, our results have important implications for the phenomenology of inclusive B -meson decays, including in particular the determination of $|V_{ub}|$. We have therefore organized the paper in such a way that the reader interested mainly in the applications of our formalism can skip the conceptual parts of the discussion in Sections 2–5 and proceed directly with Section 6, where we summarize our findings and collect all formulae needed for phenomenology. The following Sections 7, 8, and 9 contain explicit predictions for various decay rates and spectra, which are of relevance to experimenters.

During the final stages of this work, a paper by Bauer and Manohar appeared [14], which overlaps with parts of our analysis. These authors derive expressions for the hard-scattering kernels, the jet function, and the renormalized shape function which agree with our results reported in (25), (27), and (33) below. They also obtain an expression for the anomalous dimension of the shape function, which coincides with our result in (43). In many other aspects our analysis goes beyond that of [14]. In particular, using a technique published some time ago by two of us [15], we succeed to obtain an exact analytic solution of the evolution equation for the shape function in momentum space. At leading-logarithmic order we confirm an expression found earlier by Balzereit, Mannel, and Kilian (apart from a small mistake) [16]. While in [14] resummed expressions are only given for large- N moments of decay spectra, we present results for arbitrary decay distributions in physical phase space. We also disagree with Bauer and Manohar on the conclusion that moments of the renormalized shape function cannot be related to HQET parameters. In fact, we derive the explicit form of such relations.

2 Factorization theorem for inclusive decay rates

Using the optical theorem, the hadronic physics relevant to the inclusive semileptonic decay $\bar{B} \rightarrow X_u l^- \bar{\nu}$ can be related to a hadronic tensor $W^{\mu\nu}$ defined via the discontinuity of the forward B -meson matrix element of a correlator of two flavor-changing weak currents $J^\mu = \bar{u}\gamma^\mu(1 - \gamma_5)b$ [4, 5, 6]. We define

$$W^{\mu\nu} = \frac{1}{\pi} \text{Im} \frac{\langle \bar{B}(v) | T^{\mu\nu} | \bar{B}(v) \rangle}{2M_B}, \quad T^{\mu\nu} = i \int d^4x e^{iq \cdot x} \text{T} \{ J^{\dagger\mu}(0), J^\nu(x) \}. \quad (1)$$

Here v is the B -meson velocity and q the momentum carried by the lepton pair. The current correlator receives contributions from widely separated energy and distance scales. To extract the dependence on the large b -quark mass, it is convenient to rescale the heavy-quark field according to $b(x) = e^{-im_b v \cdot x} b'(x)$. The field $b'(x)$ carries the residual momentum $k = p_b - m_b v = O(\Lambda_{\text{QCD}})$. Then the phase factor in (1) becomes $e^{i(q-m_b v) \cdot x} \equiv e^{-ip \cdot x}$. In the parton model, $p = m_b v - q$ corresponds to the momentum of the jet of light partons into which the b -quark decays.

As long as at least some components of the jet momentum are large compared with Λ_{QCD} , the current correlator can be evaluated using a short-distance expansion. The simplest case arises if all components of $p^\mu \sim m_b \gg \Lambda_{\text{QCD}}$. Integrating out the light-quark propagator then produces bilocal operators of the form $\bar{b}'(x) \dots b'(0)$ with $x \sim 1/m_b$, which can be expanded in terms of local operators O_n multiplied by coefficient functions $\tilde{D}_n(m_b, v \cdot x, x^2)$. Performing the integration over x gives functions $D_n(m_b, v \cdot p, p^2) = \int d^4x e^{-ip \cdot x} \tilde{D}_n(m_b, v \cdot x, x^2)$ depending on the different short-distance scales [5, 6]. The B -meson matrix elements of the local operators O_n can be evaluated using techniques of HQET [17]. Thus, the operator product expansion produces an expansion in inverse powers of the heavy-quark mass. This expansion is relevant to the computation of inclusive decay rates without restrictive cuts on kinematic variables. Such rates are governed by parton kinematics as imprinted through the dependence on the jet momentum p . The unique operator of lowest dimension is $\bar{h}h$ (with h the effective heavy-quark field in HQET), whose forward matrix element between B -meson states is unity. The Wilson coefficient of this operator has been computed to $O(\alpha_s)$ in [18]. At next-to-leading order in the heavy-quark expansion two new operators arise, which correspond to the kinetic energy and chromo-magnetic interaction of a heavy quark. Their Wilson coefficients have been computed at tree level in [5, 6].

A more complicated situation arises in the region of phase space in which the energy of the hadronic final states is much larger than its invariant mass, meaning that some components of the vector p^μ are much larger than others. In this case, the current correlator can be expanded in non-local light-cone operators [1, 2, 3]. The formalism is most transparent when presented using the language of soft-collinear effective theory (SCET) [10]. To simplify the kinematics it is convenient to work in the B -meson rest frame, where $v^\mu = (1, 0, 0, 0)$, and to choose the lepton momentum \vec{q} along the negative z -axis, so that \vec{p} points in the z direction. Next, we define two light-like vectors $n^\mu = (1, 0, 0, 1)$ and $\bar{n}^\mu = (1, 0, 0, -1)$ satisfying $n \cdot \bar{n} = 2$, $n \cdot v = \bar{n} \cdot v = 1$. Any 4-vector can be expanded in the light-cone basis as

$$p^\mu = (n \cdot p) \frac{\bar{n}^\mu}{2} + (\bar{n} \cdot p) \frac{n^\mu}{2} + p_\perp^\mu \equiv p_+^\mu + p_-^\mu + p_\perp^\mu, \quad (2)$$

where $p_\perp \cdot n = p_\perp \cdot \bar{n} = 0$. In the shape-function region, the jet momentum (and likewise the momentum of the hadronic final state) scales like $p^\mu \sim E(\lambda, 1, \sqrt{\lambda})$, where $\lambda \sim \Lambda_{\text{QCD}}/E$ is the SCET expansion parameter and $E \sim m_b \gg \Lambda_{\text{QCD}}$. (For the jet momentum, $p_\perp = 0$ by choice of the coordinate system.) It follows that $p_-^\mu \sim E$ is a hard scale whereas $p_+^\mu \sim \Lambda_{\text{QCD}}$ is a long-distance hadronic scale. The jet invariant mass, $p^2 \sim E\Lambda_{\text{QCD}}$, defines a hybrid, intermediate short-distance scale. We refer to a momentum with these scaling properties as “hard-collinear”. The appropriate effective field theory for integrating out the short-distance fluctuations associated with the hard scale p_- is called SCET_I and has been discussed in

detail in the literature [19, 20, 21, 22]. Here we use the coordinate-space formulation of SCET developed in [22, 23].

Below a matching scale $\mu_h \sim m_b$, the semileptonic current can be expanded as

$$\bar{u}(x)\gamma^\mu(1-\gamma_5)b'(x) = \sum_{i=1}^3 \int ds \tilde{C}_i(s) \tilde{\mathcal{X}}(x+s\bar{n}) \Gamma_i^\mu \mathcal{H}(x_-) + \dots, \quad (3)$$

where the dots denote higher-order terms in the SCET expansion, which can be neglected at leading power in Λ_{QCD}/m_b . The soft heavy-quark field $\mathcal{H}(x_-) = S_s^\dagger(x_-) h(x_-)$ and the hard-collinear light-quark field $\mathcal{X}(x) = S_s^\dagger(x_-) W_{hc}^\dagger(x) \xi(x)$ are SCET building blocks that are invariant under a set of homogeneous soft and hard-collinear gauge transformations [23, 24, 25]. The objects S_s and W_{hc} are soft and hard-collinear Wilson lines [20]. Soft fields in SCET are multi-pole expanded and only depend on the minus component of the position vector x . Finally, the position-space Wilson coefficient functions $\tilde{C}_i(s)$ depend on the variable s defining the position of the hard-collinear field. Here and below we denote functions in position space with a tilde, which is omitted from the corresponding Fourier-transformed functions in momentum space. A convenient basis of Dirac structures in (3) is

$$\Gamma_1^\mu = \gamma^\mu(1-\gamma_5), \quad \Gamma_2^\mu = v^\mu(1+\gamma_5), \quad \Gamma_3^\mu = \frac{n^\mu}{n \cdot v} (1+\gamma_5). \quad (4)$$

The current correlator in (1) then becomes

$$T^{\mu\nu} = i \int d^4x e^{-ip \cdot x} \sum_{i,j=1}^3 \int ds dt \tilde{C}_j^*(t) \tilde{C}_i(s) \text{T} \{ \bar{\mathcal{H}}(0) \bar{\Gamma}_j^\mu \mathcal{X}(t\bar{n}), \tilde{\mathcal{X}}(x+s\bar{n}) \Gamma_i^\nu \mathcal{H}(x_-) \} + \dots \quad (5)$$

In a second step, the hard-collinear fluctuations associated with the light-quark jet can be integrated out by matching SCET onto HQET at an intermediate scale $\mu_i \sim \sqrt{m_b \Lambda_{\text{QCD}}}$. At leading order the SCET Lagrangian (when written in terms of the gauge-invariant fields such as \mathcal{X}) does not contain interactions between hard-collinear and soft fields. Since the external B -meson states only contain soft constituents, we can take the vacuum matrix element over the hard-collinear fields, defining a jet function

$$\langle \Omega | \text{T} \{ \mathcal{X}_k(t\bar{n}), \tilde{\mathcal{X}}_l(x+s\bar{n}) \} | \Omega \rangle \equiv \delta_{kl} \tilde{\mathcal{J}}(x + (s-t)\bar{n}) + \dots, \quad (6)$$

where k, l are color indices, and we have used translational invariance to determine the dependence on the coordinate vectors. At higher orders in SCET power counting, additional jet functions would arise, but their contributions can be neglected at leading power. Shifting the integration variable from x to $z = x + (s-t)\bar{n}$, with $z_- = x_-$, and introducing the Fourier-transformed Wilson coefficient functions

$$C_i(\bar{n} \cdot p) = \int ds e^{is\bar{n} \cdot p} \tilde{C}_i(s), \quad (7)$$

we then obtain

$$T^{\mu\nu} = i \sum_{i,j=1}^3 C_j^*(\bar{n} \cdot p) C_i(\bar{n} \cdot p) \int d^4z e^{-ip \cdot z} \bar{\mathcal{H}}(0) \bar{\Gamma}_j^\mu \tilde{\mathcal{J}}(z) \Gamma_i^\nu \mathcal{H}(z_-) + \dots \quad (8)$$

In the next step, we rewrite the bilocal heavy-quark operator as [1]

$$\begin{aligned}\bar{\mathcal{H}}(0) \Gamma \mathcal{H}(z_-) &= (\bar{h} S_s)(0) \Gamma e^{z_- \cdot \partial_+} (S_s^\dagger h)(0) = \bar{h}(0) \Gamma e^{z_- \cdot D_+} h(0) \\ &= \int d\omega e^{-\frac{i}{2}\omega \bar{n} \cdot z} \bar{h}(0) \Gamma \delta(\omega - in \cdot D) h(0),\end{aligned}\quad (9)$$

where Γ may be an arbitrary (even z -dependent) Dirac structure, and we have used the property $in \cdot D S_s = S_s in \cdot \partial$ of the soft Wilson line S_s , where $iD^\mu = i\partial^\mu + g_s A_s^\mu$ is the covariant derivative with respect to soft gauge transformations. When this expression is used in (8), the resulting formula for the correlator involves the Fourier transform of the jet function,

$$\int d^4 z e^{-ip \cdot z} \tilde{\mathcal{J}}(z) = \not{p}_- \mathcal{J}(p^2), \quad (10)$$

however with p^μ replaced by the combination $p_\omega^\mu \equiv p^\mu + \frac{1}{2}\omega \bar{n}^\mu$. In defining the momentum-space jet function $\mathcal{J}(p^2)$ we have taken into account that the matrix element in (6) vanishes when multiplied by \not{n} from either side, since $\not{n} \mathcal{X} = 0$. Using that $p_{\omega-} = p_-$, we now obtain

$$T^{\mu\nu} = i \sum_{i,j=1}^3 H_{ij}(\bar{n} \cdot p) \int d\omega \mathcal{J}(p_\omega^2) \bar{h} \bar{\Gamma}_j^\mu \not{p}_- \Gamma_i^\nu \delta(\omega - in \cdot D) h + \dots, \quad (11)$$

where $H_{ij}(\bar{n} \cdot p) = C_j^*(\bar{n} \cdot p) C_i(\bar{n} \cdot p)$ are called the hard functions.

In order to compute the hadronic tensor we take the discontinuity of the jet function,

$$J(p^2) = \frac{1}{\pi} \text{Im} [i\mathcal{J}(p^2)], \quad (12)$$

and evaluate the B -meson matrix element of the soft operator using the HQET trace formalism, which allows us to write [17]

$$\frac{\langle \bar{B}(v) | \bar{h} \Gamma \delta(\omega - in \cdot D) h | \bar{B}(v) \rangle}{2M_B} = S(\omega) \frac{1}{2} \text{tr} \left(\Gamma \frac{1 + \not{v}}{2} \right) + \dots \quad (13)$$

at leading power in the heavy-quark expansion. The soft function $S(\omega)$ coincides with the shape function $f(k_+)$ introduced in [1]. This gives the factorization formula

$$W^{\mu\nu} = \sum_{i,j=1}^3 H_{ij}(\bar{n} \cdot p) \text{tr} \left(\bar{\Gamma}_j^\mu \frac{\not{p}_-}{2} \Gamma_i^\nu \frac{1 + \not{v}}{2} \right) \int d\omega J(p_\omega^2) S(\omega) + \dots \quad (14)$$

At leading power one could replace $\not{p}_- \rightarrow \not{p}$ and $\bar{n} \cdot p = 2v \cdot p_- \rightarrow 2v \cdot p$ in this result.

In the final expressions (11) and (14) the dependence on the three scales $\bar{n} \cdot p \sim m_b$, $p_\omega^2 \sim m_b \Lambda_{\text{QCD}}$ and $\omega \sim \Lambda_{\text{QCD}}$ has been factorized into the hard, jet, and shape functions, respectively. Large logarithms associated with ratios of these scales can be resummed by solving renormalization-group equations for the scale dependence of these component functions. The factorization formula (14) was derived at tree level in [1, 2], and was generalized to all orders in perturbation theory in [8, 9]. The derivation presented above is equivalent to a proof of this

formula presented in [20] (see also [10]). The limits of integration in the convolution integral are determined by the facts that the jet function defined in (12) has support for $p_\omega^2 \geq 0$, and the shape function defined in (13) has support for $-\infty < \omega \leq \bar{\Lambda}$ with $\bar{\Lambda} = M_B - m_b$, where m_b is the heavy-quark pole mass. The argument p_ω^2 of the jet function can be rewritten as

$$p_\omega^2 = p^2 + \bar{n} \cdot p \omega = \bar{n} \cdot p (n \cdot P_H - (\bar{\Lambda} - \omega)) \equiv \bar{n} \cdot p (n \cdot P_H - \hat{\omega}), \quad (15)$$

where $P_H = M_B v - q = p + \bar{\Lambda} v$ is the 4-momentum of the hadronic final state, and the variable $\hat{\omega} = \bar{\Lambda} - \omega \geq 0$. Finally, $n \cdot P_H = E_H - |\vec{P}_H| = s_H/2E_H + O(\Lambda_{\text{QCD}}^2/m_b)$ is a kinematic variable of order Λ_{QCD} related to the hadronic invariant mass and energy of the final state. The usefulness of this variable has also been emphasized in [16, 26, 27]. We shall see below that expressing the convolution integral in terms of the new variable $\hat{\omega}$ eliminates any spurious dependence of the decay spectra on the b -quark pole mass. It follows that in the shape-function region the hadronic tensor is most naturally written as a function of the “parton variable” $\bar{n} \cdot p$ and the “hadron variable” $n \cdot P_H$, and the inclusive spectra are governed by a combination of parton and hadronic kinematics.

Using the fact that the Wilson coefficients C_i are real and hence H_{ij} is symmetric in its indices, we find

$$\begin{aligned} \sum_{i,j=1}^3 H_{ij} \text{tr} \left(\bar{\Gamma}_j^\mu \frac{\not{p}_-}{2} \Gamma_i^\nu \frac{1 + \not{p}}{2} \right) &= 2H_{11} (p_-^\mu v^\nu + p_-^\nu v^\mu - g^{\mu\nu} v \cdot p_- - i\epsilon^{\mu\nu\alpha\beta} p_{-\alpha} v_\beta) \\ &+ 2H_{22} v \cdot p_- v^\mu v^\nu + 2(H_{12} + H_{23}) (p_-^\mu v^\nu + p_-^\nu v^\mu) + 2(2H_{13} + H_{33}) \frac{p_-^\mu p_-^\nu}{v \cdot p_-}. \end{aligned} \quad (16)$$

This result may be compared with the general Lorentz decomposition of the hadronic tensor given in [18]:

$$\begin{aligned} W^{\mu\nu} &= W_1 (p_-^\mu v^\nu + p_-^\nu v^\mu - g^{\mu\nu} v \cdot p_- - i\epsilon^{\mu\nu\alpha\beta} p_{-\alpha} v_\beta) - W_2 g^{\mu\nu} \\ &+ W_3 v^\mu v^\nu + W_4 (p_-^\mu v^\nu + p_-^\nu v^\mu) + W_5 p_-^\mu p_-^\nu \end{aligned} \quad (17)$$

We see that the structure function W_2 is not generated at leading order in the SCET expansion. Since only the Wilson coefficient C_1 is non-zero at tree-level, the structure function W_1 receives leading-power contributions at tree level, whereas W_4 and W_5 receive leading-power contributions at $O(\alpha_s(m_b))$. The function W_3 receives leading-power contributions only at $O(\alpha_s^2(m_b))$, which is beyond the accuracy of a next-to-leading order calculation.

3 Matching calculations

In this section we derive perturbative expressions for the hard functions $H_{ij}(\bar{n} \cdot p)$ and the jet function $J(p_\omega^2)$ in (14) at next-to-leading order in α_s . To this end, we match expressions for the hadronic tensor obtained in full QCD, SCET, and HQET, using for simplicity on-shell external b -quark states. We also present results for the renormalized shape function in the parton model, which are needed in the matching calculation. Throughout this paper we use the $\overline{\text{MS}}$ subtraction scheme and work in $d = 4 - 2\epsilon$ space-time dimensions.

3.1 Hard functions

Perturbative expressions at $O(\alpha_s)$ for the structure functions W_i in the decomposition (17) have been obtained in [18] by evaluating one-loop Feynman graphs for the current correlator $T^{\mu\nu}$ using on-shell external quark states with residual momentum k (satisfying $v \cdot k = 0$) in full QCD. The leading terms in the region of hard-collinear jet momenta are

$$\begin{aligned}
\frac{1}{2} W_1 &= \delta(p_k^2) \left[1 - \frac{C_F \alpha_s}{4\pi} \left(8 \ln^2 y - 10 \ln y + \frac{2 \ln y}{1-y} + 4L_2(1-y) + \frac{4\pi^2}{3} + 5 \right) \right] \\
&\quad + \frac{C_F \alpha_s}{4\pi} \left[-4 \left(\frac{\ln(p_k^2/m_b^2)}{p_k^2} \right)_*^{[m_b^2]} + (8 \ln y - 7) \left(\frac{1}{p_k^2} \right)_*^{[m_b^2]} \right] + \dots, \\
\frac{1}{2} W_4 &= \delta(p_k^2) \frac{C_F \alpha_s}{4\pi} \frac{2}{1-y} \left(\frac{y \ln y}{1-y} + 1 \right) + \dots, \\
\frac{m_b}{4} W_5 &= \delta(p_k^2) \frac{C_F \alpha_s}{4\pi} \frac{2}{1-y} \left(\frac{1-2y}{1-y} \ln y - 1 \right) + \dots,
\end{aligned} \tag{18}$$

whereas W_2 and W_3 do not receive leading-power contributions at this order, in accordance with our general observations made above. Here $\alpha_s \equiv \alpha_s(\mu)$, $y = \bar{n} \cdot p / m_b$, and $p_k^2 = p^2 + \bar{n} \cdot p \, n \cdot k$. We have used that $2v \cdot p / m_b = \bar{n} \cdot p / m_b + O(\lambda)$ in the hard-collinear region. The star distributions are generalized plus distributions defined as [18]

$$\begin{aligned}
\int_{\leq 0}^z dx F(x) \left(\frac{1}{x} \right)_*^{[u]} &= \int_0^z dx \frac{F(x) - F(0)}{x} + F(0) \ln \frac{z}{u}, \\
\int_{\leq 0}^z dx F(x) \left(\frac{\ln(x/u)}{x} \right)_*^{[u]} &= \int_0^z dx \frac{F(x) - F(0)}{x} \ln \frac{x}{u} + \frac{F(0)}{2} \ln^2 \frac{z}{u},
\end{aligned} \tag{19}$$

where $F(x)$ is a smooth test function. For later purposes, we note the useful identities

$$\begin{aligned}
\lambda \left(\frac{1}{\lambda x} \right)_*^{[u]} &= \left(\frac{1}{x} \right)_*^{[u/\lambda]} = \left(\frac{1}{x} \right)_*^{[u]} + \delta(x) \ln \lambda, \\
\lambda \left(\frac{\ln(\lambda x/u)}{\lambda x} \right)_*^{[u]} &= \left(\frac{\ln(\lambda x/u)}{x} \right)_*^{[u/\lambda]} = \left(\frac{\ln(x/u)}{x} \right)_*^{[u]} + \left(\frac{1}{x} \right)_*^{[u]} \ln \lambda + \frac{\delta(x)}{2} \ln^2 \lambda.
\end{aligned} \tag{20}$$

In order to find the hard functions H_{ij} , we calculate the discontinuity of the current correlator (5) between on-shell heavy-quark states in momentum space. We work to one-loop order in SCET, keeping i, j fixed and omitting the Wilson coefficient functions. The corresponding tree diagram yields

$$D^{(0)} = K \delta(p_k^2), \quad \text{with} \quad K = \bar{u}_b(v) \bar{\Gamma}_j^\mu \not{p}_- \Gamma_i^\nu u_b(v), \tag{21}$$

where $u_b(v)$ are on-shell HQET spinors normalized to unity, and the quantity K corresponds to the Dirac trace in (14). The interpretation of this result in terms of hard, jet, and soft

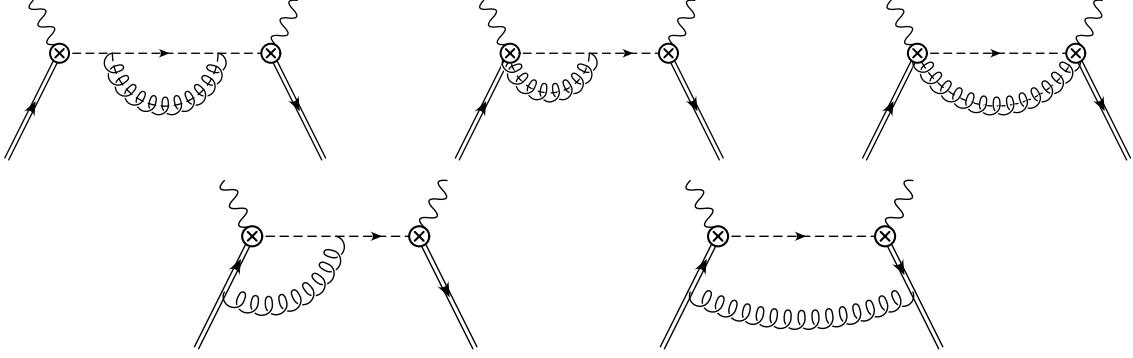


Figure 1: One-loop diagrams contributing to the current correlator in SCET. The effective current operators are denoted by crossed circles, and hard-collinear propagators are drawn as dashed lines. Mirror graphs obtained by exchanging the two currents are not shown.

functions is that, at tree level, $J^{(0)}(p_\omega^2) = \delta(p_\omega^2)$ and $S_{\text{parton}}^{(0)}(\omega) = \delta(\omega - n \cdot k)$. (The second result is specific to the free-quark decay picture.) Then the convolution integral $\int d\omega J(p_\omega^2) S(\omega)$ in (14) produces $\delta(p_k^2)$, and comparison with (18) shows that $H_{11}^{(0)} = 1$, while all other hard functions vanish at tree level.

The diagrams contributing at one-loop order are shown in Figure 1. They are evaluated using the Feynman rules of SCET. The first three graphs contain hard-collinear gluon exchanges, while the last two diagrams contain soft exchanges. The wave-function renormalization factors of the external heavy quarks equal 1 on-shell. For the sum of all hard-collinear exchange graphs, we find

$$D_{hc}^{(1)} = K \frac{C_F \alpha_s}{4\pi} \left[\left(\frac{4}{\epsilon^2} + \frac{3}{\epsilon} + 7 - \pi^2 \right) \delta(p_k^2) + 4 \left(\frac{\ln(p_k^2/\mu^2)}{p_k^2} \right)_*^{[\mu^2]} - \left(\frac{4}{\epsilon} + 3 \right) \left(\frac{1}{p_k^2} \right)_*^{[\mu^2]} \right]. \quad (22)$$

The sum of the soft contributions is given by

$$D_s^{(1)} = K \frac{C_F \alpha_s}{4\pi} \left[\left(-\frac{2}{\epsilon^2} - \frac{4}{\epsilon} L + \frac{2}{\epsilon} - 4L^2 + 4L - \frac{\pi^2}{6} \right) \delta(p_k^2) - 8 \left(\frac{\ln(p_k^2/\mu^2)}{p_k^2} \right)_*^{[\mu^2]} + \left(\frac{4}{\epsilon} + 8L - 4 \right) \left(\frac{1}{p_k^2} \right)_*^{[\mu^2]} \right], \quad (23)$$

where $L = \ln(\bar{n} \cdot p/\mu)$. The $1/\epsilon$ poles in the sum of the hard-collinear and soft contributions are subtracted by a multiplicative renormalization factor Z_J^2 applied to the bare current correlator in (5), where

$$Z_J = 1 + \frac{C_F \alpha_s}{4\pi} \left(-\frac{1}{\epsilon^2} + \frac{2}{\epsilon} L - \frac{5}{2\epsilon} \right) \quad (24)$$

is the (momentum-space) current renormalization constant in SCET [19]. Taking the sum of (22) and (23) after subtraction of the pole terms, and matching it with the results in (18), we

find that at one-loop order

$$\begin{aligned}
H_{11}(\bar{n} \cdot p) &= 1 + \frac{C_F \alpha_s}{4\pi} \left(-4L^2 + 10L - 4 \ln y - \frac{2 \ln y}{1-y} - 4L_2(1-y) - \frac{\pi^2}{6} - 12 \right), \\
H_{12}(\bar{n} \cdot p) &= \frac{C_F \alpha_s}{4\pi} \frac{2}{1-y} \left(\frac{y \ln y}{1-y} + 1 \right), \\
H_{13}(\bar{n} \cdot p) &= \frac{C_F \alpha_s}{4\pi} \frac{y}{1-y} \left(\frac{1-2y}{1-y} \ln y - 1 \right).
\end{aligned} \tag{25}$$

In deriving these results we have used the identities (20) to rearrange the various star distributions. The remaining hard functions start at $O(\alpha_s^2)$. Using the relation $H_{ij} = C_i C_j$, one can derive from these results expressions for the Wilson coefficients in the expansion of the semileptonic current in (3). We confirm the expressions for these coefficients given in [19].

3.2 Jet function

After the hadronic tensor is matched onto HQET as shown in (14), the SCET loop graphs in Figure 1 determine the one-loop contributions to the product of the jet function and the shape function in (14). We may write this product symbolically as $J^{(1)} \otimes S^{(0)} + J^{(0)} \otimes S^{(1)}$, where the \otimes symbol means a convolution in ω . Whereas the jet function is a short-distance object that can be calculated in perturbation theory, the shape function is defined in terms of a hadronic matrix element and cannot be properly described using Feynman diagrams with on-shell external quark states. In a second step, we must therefore extract from the results (22) and (23) the one-loop contribution $J^{(1)}$ to the jet function. To this end, we must compute the renormalized shape function at one-loop order in the parton model. This will be done in the next subsection. We may, however, already anticipate the result for the jet function at this point, because at one-loop order the graphs in Figure 1 can be separated into diagrams with hard-collinear (first line) or soft (second line) gluon exchange. (This separation would be non-trivial beyond one-loop order.) The hard-collinear contribution in (22) thus determines the convolution $J^{(1)} \otimes S^{(0)} = J^{(1)}(p_k^2)$, whereas the soft contribution in (23) corresponds to $J^{(0)} \otimes S^{(1)}$. It follows that the renormalized jet function is given by the distribution

$$J(p_\omega^2) = \delta(p_\omega^2) + \frac{C_F \alpha_s}{4\pi} \left[(7 - \pi^2) \delta(p_\omega^2) + 4 \left(\frac{\ln(p_\omega^2/\mu^2)}{p_\omega^2} \right)_*^{[\mu^2]} - 3 \left(\frac{1}{p_\omega^2} \right)_*^{[\mu^2]} \right]. \tag{26}$$

This result disagrees with a corresponding expression obtained in [28]. It will often be useful to separate the dependence on $\bar{n} \cdot p$ and $n \cdot P_H$ in this result by means of the substitution $p_\omega^2 = y \hat{p}_\omega^2$, where $\hat{p}_\omega^2 = m_b(n \cdot P_H - \hat{\omega})$ according to (15). Using the identities (20), we find

$$\begin{aligned}
y J(p_\omega^2) \equiv \hat{J}(\hat{p}_\omega^2, y) &= \delta(\hat{p}_\omega^2) + \frac{C_F \alpha_s}{4\pi} \left[(2 \ln^2 y - 3 \ln y + 7 - \pi^2) \delta(\hat{p}_\omega^2) \right. \\
&\quad \left. + 4 \left(\frac{\ln(\hat{p}_\omega^2/\mu^2)}{\hat{p}_\omega^2} \right)_*^{[\mu^2]} + (4 \ln y - 3) \left(\frac{1}{\hat{p}_\omega^2} \right)_*^{[\mu^2]} \right].
\end{aligned} \tag{27}$$

The jet function is non-zero only if $y \geq 0$ and $n \cdot P_H \geq \hat{\omega}$, which ensures that $p_\omega^2 \geq 0$.

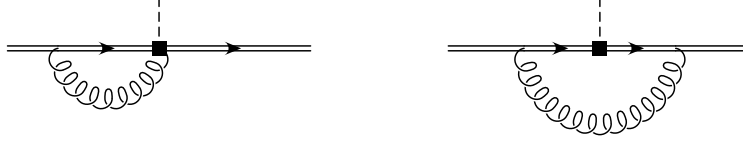


Figure 2: Radiative corrections to the shape function. The bilocal HQET operator is denoted by the black square. A mirror copy of the first graph is not shown.

3.3 Renormalized shape function

Having calculated the short-distance objects H_{ij} and J in the factorization formula (14) at one-loop order, we now turn to a study of radiative corrections to the shape function $S(\omega)$. There is considerable confusion in the literature about the renormalization properties of the shape function, and several incorrect results for its anomalous dimension have been published. We therefore present our calculation in some detail in this subsection and the following section.

According to (13), the shape function is defined in terms of a hadronic matrix element in HQET and thus cannot be calculated perturbatively. However, the renormalization properties of this function can be studied using perturbation theory. To this end, we evaluate the matrix element (13) in HQET using external heavy-quark states with residual momentum k . For the time being, we keep $v \cdot k$ non-zero to regularize infra-red singularities. The relevant one-loop graphs are depicted in Figure 2. Adding the tree contribution, we obtain for the matrix element of the bare shape-function operator $O(\omega) = \bar{h} \Gamma \delta(\omega - in \cdot D) h$ (expressed in terms of renormalized fields)

$$\begin{aligned}
S_{\text{bare}}(\omega) = & Z_h \delta(\omega - n \cdot k) - \frac{4C_F g_s^2}{(4\pi)^{2-\epsilon}} \Gamma(1 + \epsilon) \\
& \times \left\{ \frac{1}{\epsilon} \int_0^\infty dl l^{-1-2\epsilon} \left[\delta(\omega - n \cdot k) - \delta(\omega - n \cdot k + l) \right] \left(1 + \frac{\delta}{l} \right)^{-\epsilon} \right. \\
& \left. + \theta(n \cdot k - \omega) (n \cdot k - \omega)^{-\epsilon} (n \cdot k - \omega + \delta)^{-1-\epsilon} \right\}, \tag{28}
\end{aligned}$$

where $\delta = -2v \cdot k$, and

$$Z_h = 1 + \frac{4C_F g_s^2}{(4\pi)^{2-\epsilon}} \Gamma(2\epsilon) \Gamma(1 - \epsilon) \delta^{-2\epsilon} \tag{29}$$

is the off-shell wave-function renormalization constant of a heavy quark in HQET. The next step is to extract the ultra-violet poles from this result, which determine the anomalous dimension of the shape function. We define a renormalization factor through

$$\begin{aligned}
S_{\text{ren}}(\omega) &= \int_{-\infty}^{\bar{\Lambda}} d\omega' Z_S(\omega, \omega') S_{\text{bare}}(\omega'), \\
Z_S(\omega, \omega') &= \delta(\omega - \omega') + \frac{C_F \alpha_s}{4\pi} z_S(\omega, \omega') + \dots \tag{30}
\end{aligned}$$

The result for Z_S following from (28) must be interpreted as a distribution on test functions $F(\omega')$ with support on the interval $-\infty < \omega' \leq \bar{\Lambda}$. We obtain

$$\begin{aligned} z_S(\omega, \omega') &= \left(\frac{2}{\epsilon^2} + \frac{4}{\epsilon} \ln \frac{\mu}{\bar{\Lambda} - \omega} - \frac{2}{\epsilon} \right) \delta(\omega - \omega') - \frac{4}{\epsilon} \left(\frac{\theta(\omega' - \omega)}{\omega' - \omega} \right)_+ \\ &= \left(\frac{2}{\epsilon^2} - \frac{2}{\epsilon} \right) \delta(\omega - \omega') - \frac{4}{\epsilon} \left(\frac{1}{\omega' - \omega} \right)_*^{[\mu]}. \end{aligned} \quad (31)$$

Note the peculiar dependence on the parameter $\bar{\Lambda}$ setting the upper limit on the integration over ω' in (30), which combines with the plus distribution to form a star distribution in the variable $(\omega' - \omega)$.

We can now determine the renormalized shape function from (30). The result must once again be interpreted as a distribution, this time on test functions $F(\omega)$ integrated over a *finite* interval $-\Lambda_{\text{had}} \leq \omega \leq \bar{\Lambda}$. In practice, the value of Λ_{had} is set by kinematics or by virtue of some experimental cut (see Sections 7 and 9 below). The result is

$$\begin{aligned} S_{\text{parton}}(\omega) &= \delta(\omega - n \cdot k) \left\{ 1 - \frac{C_F \alpha_s}{\pi} \left[\frac{\pi^2}{24} + L_2 \left(\frac{-\delta}{\Lambda_{\text{had}} + n \cdot k} \right) \right] \right\} \\ &\quad - \frac{C_F \alpha_s}{\pi} \left\{ \left[\frac{\theta(n \cdot k - \omega)}{n \cdot k - \omega} \left(\ln \frac{n \cdot k - \omega}{\mu} + \ln \frac{n \cdot k - \omega + \delta}{\mu} \right) \right]_+ \right. \\ &\quad \left. + \delta(n \cdot k - \omega) \ln^2 \frac{\Lambda_{\text{had}} + n \cdot k}{\mu} + \frac{\theta(n \cdot k - \omega)}{n \cdot k - \omega + \delta} + \delta(n \cdot k - \omega) \ln \frac{\delta}{\mu} \right\}. \end{aligned} \quad (32)$$

While it was useful to keep the heavy quark off-shell in the calculation of the ultra-violet renormalization factor, the limit $\delta = -2v \cdot k \rightarrow 0$ can be taken in the result for the renormalized shape functions without leading to infra-red singularities. This gives

$$\begin{aligned} S_{\text{parton}}(\omega) &= \delta(\omega - n \cdot k) \left(1 - \frac{C_F \alpha_s}{\pi} \frac{\pi^2}{24} \right) \\ &\quad - \frac{C_F \alpha_s}{\pi} \left[2 \left(\frac{1}{n \cdot k - \omega} \ln \frac{n \cdot k - \omega}{\mu} \right)_*^{[\mu]} + \left(\frac{1}{n \cdot k - \omega} \right)_*^{[\mu]} \right], \end{aligned} \quad (33)$$

where the star distributions must now be understood as distributions in the variable $(n \cdot k - \omega)$.

We stress that these results for the renormalized shape function are obtained in the parton model and can in no way provide a realistic prediction for the functional form of $S(\omega)$. This should be obvious from the fact that our results depend on a single “hadronic parameter” $n \cdot k$, corresponding to a fixed residual momentum of the heavy quark. Only the dependence on the ultra-violet renormalization scale μ can be trusted. However, the one-loop result in (33) is needed to complete the matching calculation of the jet function described in the previous subsection, which can legitimately be performed with on-shell external b -quark states. Given

the expression for the renormalized shape function, we obtain

$$\begin{aligned} \int d\omega J^{(0)}(p_\omega^2) S^{(1)}(\omega) &= \frac{1}{\bar{n} \cdot p} S^{(1)}(-p^2/\bar{n} \cdot p) \\ &= -\frac{C_F \alpha_s}{\pi} \left[\frac{\pi^2}{24} \delta(p_k^2) + \frac{2}{\bar{n} \cdot p} \left(\frac{\bar{n} \cdot p}{p_k^2} \ln \frac{p_k^2}{\bar{n} \cdot p \mu} \right)_*^{[\mu]} + \frac{1}{\bar{n} \cdot p} \left(\frac{\bar{n} \cdot p}{p_k^2} \right)_*^{[\mu]} \right]. \end{aligned} \quad (34)$$

With the help of the identities (20) this can be shown to be equal to the finite part of (23), as we claimed above.

4 Renormalization-group resummation

Equations (25) and (26) determine the short-distance objects H_{ij} and J in the factorization formula (14) at one-loop order in perturbation theory. However, there is no common choice of the renormalization scale μ that would eliminate all large logarithms from these results. Likewise, the shape function, being a hadronic matrix element, is naturally renormalized at some low scale, whereas the short-distance objects contain physics at higher scales. The problem of large logarithms arising from the presence of disparate mass scales can be dealt with using renormalization-group equations. Proceeding in three steps, our strategy will be as follows:

i) At a high scale $\mu_h \sim m_b$ we match QCD onto SCET and extract matching conditions for the hard functions H_{ij} . The corresponding one-loop expressions have been given in (25). At that scale, they are free of large logarithms and so can be reliably computed using perturbation theory. We then evolve the hard functions down to an intermediate hard-collinear scale $\mu_i \sim \sqrt{m_b \Lambda_{\text{QCD}}}$ by solving the renormalization-group equation

$$\frac{d}{d \ln \mu} H_{ij}(\bar{n} \cdot p, \mu) = 2\gamma_J(\bar{n} \cdot p, \mu) H_{ij}(\bar{n} \cdot p, \mu), \quad (35)$$

where γ_J is the anomalous dimension of the semileptonic current in SCET.

ii) Next, we start from a model for the shape function $S(\omega, \mu_0)$ at some low scale $\mu_0 = \text{few} \times \Lambda_{\text{QCD}}$ large enough to trust perturbation theory. Such a model could be provided by a QCD-inspired approach such as QCD sum rules or lattice QCD, or it could be tuned to experimental data. We then solve the integro-differential evolution equation

$$\frac{d}{d \ln \mu} S(\omega, \mu) = - \int d\omega' \gamma_S(\omega, \omega', \mu) S(\omega', \mu) \quad (36)$$

to obtain the shape function at the intermediate scale μ_i .

iii) Finally, at the scale μ_i we combine the results for the hard functions and for the shape function with the jet function J in (26), which at that scale is free of large logarithms and so has a reliable perturbative expansion. The dependence on the matching scales μ_h and μ_i cancels in the final result (to the order at which we are working).

We now discuss these three steps in detail.

4.1 Evolution of the hard functions

At one-loop order, the anomalous dimension γ_J for the SCET current is twice the coefficient of the $1/\epsilon$ pole in the renormalization factor Z_J in (24). More generally [19, 29],

$$\gamma_J(\bar{n} \cdot p, \mu) = -\Gamma_{\text{cusp}}(\alpha_s) \ln \frac{\mu}{\bar{n} \cdot p} + \gamma'(\alpha_s) = \frac{C_F \alpha_s}{\pi} \left(-\ln \frac{\mu}{\bar{n} \cdot p} - \frac{5}{4} \right) + \dots, \quad (37)$$

where $\Gamma_{\text{cusp}} = C_F \alpha_s / \pi + \dots$ is the universal cusp anomalous dimension governing the ultra-violet singularities of Wilson lines with light-like segments [30]. The exact solution to the evolution equation (35) can be written as

$$H_{ij}(\bar{n} \cdot p, \mu_i) = H_{ij}(\bar{n} \cdot p, \mu_h) \exp U_H(\bar{n} \cdot p, \mu_h, \mu_i), \quad (38)$$

where

$$U_H(\bar{n} \cdot p, \mu_h, \mu_i) = 2 \int_{\alpha_s(\mu_h)}^{\alpha_s(\mu_i)} \frac{d\alpha}{\beta(\alpha)} \left[\Gamma_{\text{cusp}}(\alpha) \left(\ln \frac{\bar{n} \cdot p}{\mu_h} - \int_{\alpha_s(\mu_h)}^{\alpha} \frac{d\alpha'}{\beta(\alpha')} \right) + \gamma'(\alpha) \right], \quad (39)$$

and $\beta(\alpha_s) = d\alpha_s/d\ln\mu$ is the QCD β -function. Defining as usual

$$\Gamma_{\text{cusp}}(\alpha_s) = \sum_{n=0}^{\infty} \Gamma_n \left(\frac{\alpha_s}{4\pi} \right)^{n+1}, \quad \beta(\alpha_s) = -2\alpha_s \sum_{n=0}^{\infty} \beta_n \left(\frac{\alpha_s}{4\pi} \right)^{n+1}, \quad (40)$$

and similarly for all other anomalous dimensions, setting $r_1 = \alpha_s(\mu_i)/\alpha_s(\mu_h) > 1$, and expanding the evolution function to $O(\alpha_s)$, we obtain

$$e^{U_H(\bar{n} \cdot p, \mu_h, \mu_i)} = e^{V_H(\mu_h, \mu_i)} \left(\frac{\bar{n} \cdot p}{\mu_h} \right)^{-\frac{\Gamma_0}{\beta_0} \ln r_1} \left[1 - \frac{\alpha_s(\mu_h)}{4\pi} \frac{\Gamma_0}{\beta_0} \left(\frac{\Gamma_1}{\Gamma_0} - \frac{\beta_1}{\beta_0} \right) (r_1 - 1) \ln \frac{\bar{n} \cdot p}{\mu_h} \right], \quad (41)$$

where

$$V_H(\mu_h, \mu_i) = \frac{\Gamma_0}{2\beta_0^2} \left[\frac{4\pi}{\alpha_s(\mu_h)} \left(1 - \frac{1}{r_1} - \ln r_1 \right) + \frac{\beta_1}{2\beta_0} \ln^2 r_1 - \left(\frac{\Gamma_1}{\Gamma_0} - \frac{\beta_1}{\beta_0} \right) (r_1 - 1 - \ln r_1) \right] - \frac{\gamma'_0}{\beta_0} \ln r_1 + O[(r_1 - 1) \alpha_s(\mu_h)]. \quad (42)$$

Let us briefly explain the structure of resummed perturbation theory in applications with Sudakov double logarithms. In renormalization-group improved perturbation theory the parameter r_1 is treated as a quantity of $O(1)$. The terms proportional to $1/\alpha_s(\mu_h)$ in V_H resum the leading, double logarithmic terms to all orders in perturbation theory. The remaining $O(1)$ terms in V_H contribute at leading, single-logarithmic order. Note that these effects are not suppressed by any small parameter. We therefore refer to the combination of these two terms as the “leading order”. At next-to-leading order, the corrections proportional to the coupling $\alpha_s(\mu_h)$ are included. In our case, the only piece missing for a complete resummation at next-to-leading order is the $O(\alpha_s)$ contribution to V_H , which is independent of the

kinematic variable $\bar{n} \cdot p$ and vanishes for $\mu_i \rightarrow \mu_h$. To compute these terms would require to calculate the cusp anomalous dimension to three loops and the anomalous dimension γ' to two loops. The fact that the corresponding expansion coefficients are unknown implies a universal, process-independent small uncertainty in the normalization of inclusive B -decay spectra in the shape-function region. We stress, however, that this uncertainty cancels in all ratios of decay distributions, even between $\bar{B} \rightarrow X_u l^- \bar{\nu}$ and $\bar{B} \rightarrow X_s \gamma$ spectra.

In phenomenological applications of our results the intermediate scale μ_i will be of order m_c , because a restriction to hadronic invariant masses below the charm threshold is used to separate $\bar{B} \rightarrow X_u l^- \bar{\nu}$ from $\bar{B} \rightarrow X_c l^- \bar{\nu}$ decays. It is then appropriate to perform the running between μ_h and μ_i in a theory with $n_f = 4$ light quark flavors. The relevant expansion coefficients are $\Gamma_0 = \frac{16}{3}$, $\Gamma_1 = \frac{2576}{27} - \frac{16}{3}\pi^2$, $\gamma'_0 = -\frac{20}{3}$, and $\beta_0 = \frac{25}{3}$, $\beta_1 = \frac{154}{3}$.

4.2 Evolution of the shape function

At one-loop order, the anomalous dimension for the shape function is twice the coefficient of the $1/\epsilon$ pole in the renormalization factor Z_S . From (31), we obtain

$$\gamma_S(\omega, \omega', \mu) = \frac{C_F \alpha_s}{\pi} \left[\left(2 \ln \frac{\mu}{\bar{\Lambda} - \omega} - 1 \right) \delta(\omega - \omega') - 2 \left(\frac{\theta(\omega' - \omega)}{\omega' - \omega} \right)_+ \right]. \quad (43)$$

Let us briefly compare this result with previous calculations of this anomalous dimension published in the literature. In [16], Balzereit et al. obtained a result that almost agrees with ours, except for the factors of 2 in front of the logarithmic term and of the plus distribution. (Their expression is, however, given in a rather different form.) Aglietti and Ricciardi tried to extract the renormalized shape function by matching QCD directly onto HQET, without including a jet function [31]. They obtained results for the renormalization factor Z_S (and hence for the anomalous dimension) in two different regularization schemes. Their expression obtained in dimensional regularization disagrees with our findings. Bauer et al. computed the anomalous dimension of the shape function using SCET [10]. They interpreted the renormalization factor in (31) as a distribution in ω rather than ω' and studied the renormalization-group equation for the short-distance coefficients $H_{ij} \cdot J$ instead of that for the shape function. If this is done, the logarithm in the anomalous dimension in (43) must be replaced by $\ln[\mu/(\Lambda_{\text{had}} + \omega')]$, where Λ_{had} is the lower cutoff on the integral over ω (see the discussion in Section 3.3). The value of this cutoff is process dependent and set by kinematics or by virtue of some experimental cut. In the shape-function region, $\Lambda_{\text{had}} = O(\Lambda_{\text{QCD}})$. Instead, in [10] the combination $(\Lambda_{\text{had}} + \omega')$ is identified with the b -quark mass, which is incorrect.

The evolution equation (36) can be solved analytically using a general method developed in [15]. It is convenient to change variables from ω to $\hat{\omega} = \bar{\Lambda} - \omega \in [0, \infty[$ and denote $\hat{S}(\hat{\omega}) \equiv S(\bar{\Lambda} - \hat{\omega})$. The renormalization-group equation then reads

$$\frac{d}{d \ln \mu} \hat{S}(\hat{\omega}, \mu) = - \int_0^\infty d\hat{\omega}' \hat{\gamma}_S(\hat{\omega}, \hat{\omega}', \mu) \hat{S}(\hat{\omega}', \mu), \quad (44)$$

where the anomalous dimension can be written in the general form

$$\hat{\gamma}_S(\hat{\omega}, \hat{\omega}', \mu) = 2 \left[\Gamma_{\text{cusp}}(\alpha_s) \ln \frac{\mu}{\hat{\omega}} + \gamma(\alpha_s) \right] \delta(\hat{\omega} - \hat{\omega}') + 2\mathcal{G}(\hat{\omega}, \hat{\omega}', \alpha_s). \quad (45)$$

The logarithmic term containing the cusp anomalous dimension has a geometric origin. Since the heavy-quark field $h(x)$ in HQET can be represented as a Wilson line along the v direction, the field $\mathcal{H}(x)$ entering the SCET formalism contains the product of a light-like Wilson line (along n) and a time-like Wilson line (along v), which form a cusp at point x . The shape function contains two such cusps. According to the renormalization theory of Wilson lines with light-like segments, each cusp produces a contribution to the anomalous dimension proportional to $\Gamma_{\text{cusp}} \ln \mu$ [30]. The one-loop coefficients of the remaining terms in (45) are

$$\gamma_0 = -2C_F, \quad \mathcal{G}_0(\hat{\omega}, \hat{\omega}') = -\Gamma_0 \left(\frac{\theta(\hat{\omega} - \hat{\omega}')}{\hat{\omega} - \hat{\omega}'} \right)_+. \quad (46)$$

The general solution of (44) can be obtained using the fact that on dimensional grounds

$$\int_0^\infty d\hat{\omega}' \mathcal{G}(\hat{\omega}, \hat{\omega}', \alpha_s) (\hat{\omega}')^a \equiv \hat{\omega}^a \mathcal{F}(a, \alpha_s), \quad (47)$$

where the function \mathcal{F} only depends on the exponent a and the coupling constant. We set $\mathcal{F}(0, \alpha_s) = 0$ by definition, thereby determining the split between the terms with γ and \mathcal{G} in (45). The integral on the left-hand side is convergent as long as $\text{Re } a > -1$. At one-loop order we find from (46)

$$\mathcal{F}(a, \alpha_s) = \Gamma_0 \frac{\alpha_s}{4\pi} \left[\psi(1+a) + \gamma_E \right] + \dots, \quad (48)$$

where $\psi(z)$ is the logarithmic derivative of the Euler Γ function. Relation (47) implies that the ansatz [15]

$$f(\hat{\omega}, \mu, \mu_0, \tau) = \left(\frac{\hat{\omega}}{\mu_0} \right)^{\tau + 2g(\mu, \mu_0)} \exp U_S(\tau, \mu, \mu_0) \quad (49)$$

with

$$g(\mu, \mu_0) = \int_{\alpha_s(\mu_0)}^{\alpha_s(\mu)} d\alpha \frac{\Gamma_{\text{cusp}}(\alpha)}{\beta(\alpha)}, \quad (50)$$

$$U_S(\tau, \mu, \mu_0) = -2 \int_{\alpha_s(\mu_0)}^{\alpha_s(\mu)} \frac{d\alpha}{\beta(\alpha)} \left[g(\mu, \mu_\alpha) + \gamma(\alpha) + \mathcal{F}(\tau + 2g(\mu_\alpha, \mu_0), \alpha) \right],$$

provides a solution to the evolution equation (44) with initial condition $f(\hat{\omega}, \mu_0, \mu_0, \tau) = (\hat{\omega}/\mu_0)^\tau$ at some scale μ_0 . Here μ_α is defined such that $\alpha_s(\mu_\alpha) = \alpha$, and τ can be an arbitrary complex parameter. Note that $g(\mu, \mu_0) > 0$ if $\mu > \mu_0$. We now assume that the shape function $\hat{S}(\hat{\omega}, \mu_0)$ is given at the low scale μ_0 and define its Fourier transform with respect to $\ln(\hat{\omega}/\mu_0)$ through

$$\hat{S}(\hat{\omega}, \mu_0) = \frac{1}{2\pi} \int_{-\infty}^{\infty} dt \mathcal{S}_0(t) \left(\frac{\hat{\omega}}{\mu_0} \right)^{it}. \quad (51)$$

The exact result for the shape function at a different scale μ is then given by

$$\hat{S}(\hat{\omega}, \mu) = \frac{1}{2\pi} \int_{-\infty}^{\infty} dt \mathcal{S}_0(t) f(\hat{\omega}, \mu, \mu_0, it). \quad (52)$$

With the help of this formula, it is straightforward to derive explicit expressions for the evolution of the shape function from the hadronic scale μ_0 up to the intermediate scale μ_i at any order in renormalization-group improved perturbation theory. Setting $r_2 = \alpha_s(\mu_0)/\alpha_s(\mu_i) > 1$, we obtain for the evolution function at leading order

$$f(\hat{\omega}, \mu_i, \mu_0, it) = e^{V_S(\mu_i, \mu_0)} \left(\frac{\hat{\omega}}{\mu_0} \right)^{it + \frac{\Gamma_0}{\beta_0} \ln r_2} \frac{\Gamma(1+it)}{\Gamma(1+it + \frac{\Gamma_0}{\beta_0} \ln r_2)}, \quad (53)$$

where

$$V_S(\mu_i, \mu_0) = \frac{\Gamma_0}{2\beta_0^2} \left[-\frac{4\pi}{\alpha_s(\mu_0)} (r_2 - 1 - \ln r_2) + \frac{\beta_1}{2\beta_0} \ln^2 r_2 + \left(\frac{\Gamma_1}{\Gamma_0} - \frac{\beta_1}{\beta_0} \right) \left(1 - \frac{1}{r_2} - \ln r_2 \right) \right] \\ - \frac{\Gamma_0}{\beta_0} \gamma_E \ln r_2 - \frac{\gamma_0}{\beta_0} \ln r_2 + O[(r_2 - 1) \alpha_s(\mu)]. \quad (54)$$

This result is valid as long as $(\Gamma_0/\beta_0) \ln r_2 < 1$, which is the case for all reasonable parameter values. Missing for a resummation at next-to-leading order are the $O(\alpha_s)$ contributions to V_S , which vanish for $\mu \rightarrow \mu_0$. Since these corrections have an unknown dependence on t via the two-loop contribution to the function $\mathcal{F}(\alpha_s, a)$, they will affect the $\hat{\omega}$ dependence of the final result. There are also some known $O(\alpha_s)$ corrections to (53) proportional to $\ln(\hat{\omega}/\mu_0)$, which we have omitted for consistency. For all practical purposes, given the intrinsic uncertainties in our knowledge of the shape function, it will be sufficient to use the equations given above. As mentioned earlier, we typically have $\mu_i \sim m_c$, and so the running between μ_i and μ_0 should be performed in a theory with $n_f = 3$ light quark flavors. The relevant expansion coefficients are then $\Gamma_0 = \frac{16}{3}$, $\Gamma_1 = \frac{304}{3} - \frac{16}{3}\pi^2$, $\gamma_0 = -\frac{8}{3}$, and $\beta_0 = 9$, $\beta_1 = 64$.

The leading-order result presented above can be simplified further. When (53) is inserted into (52), the integration over t can be performed analytically. Setting $\eta = (\Gamma_0/\beta_0) \ln r_2 > 0$, the relevant integral is

$$I = \frac{1}{2\pi} \int_{-\infty}^{\infty} dt \mathcal{S}_0(t) \left(\frac{\hat{\omega}}{\mu_0} \right)^{it} \frac{\Gamma(1+it)}{\Gamma(1+it+\eta)}, \quad (55)$$

where

$$\mathcal{S}_0(t) = \int_0^{\hat{\omega}} \frac{d\hat{\omega}'}{\hat{\omega}'} \hat{S}(\hat{\omega}', \mu_0) \left(\frac{\hat{\omega}'}{\mu_0} \right)^{-it} \quad (56)$$

is the Fourier transform of the shape function as defined in (51). The integrand of the t -integral has poles on the positive imaginary axis located at $t = in$ with $n \geq 1$ an integer. For $\hat{\omega} < \hat{\omega}'$ the integration contour can be closed in the lower half-plane avoiding all poles, hence yielding zero. For $\hat{\omega} > \hat{\omega}'$ we use the theorem of residues to obtain

$$I = \int_0^{\hat{\omega}} d\hat{\omega}' R(\hat{\omega}, \hat{\omega}') \hat{S}(\hat{\omega}', \mu_0), \quad (57)$$

where

$$R(\hat{\omega}, \hat{\omega}') = \frac{1}{\hat{\omega}} \sum_{j=0}^{\infty} \left(-\frac{\hat{\omega}'}{\hat{\omega}} \right)^j \frac{1}{\Gamma(j+1) \Gamma(\eta-j)} = \frac{1}{\Gamma(\eta)} \frac{1}{\hat{\omega}^\eta (\hat{\omega} - \hat{\omega}')^{1-\eta}}. \quad (58)$$

Note that $R(\hat{\omega}, \hat{\omega}') \rightarrow \delta(\hat{\omega} - \hat{\omega}')$ in the limit $\eta \rightarrow 0$, corresponding to $\mu_i \rightarrow \mu_0$, as it should be. Our final result for the shape function at the intermediate hard-collinear scale, valid at leading order in renormalization-group improved perturbation theory, can now be written in the simple form (valid for $\mu_i > \mu_0$, so that $\eta > 0$)

$$\hat{S}(\hat{\omega}, \mu_i) = e^{V_S(\mu_i, \mu_0)} \frac{1}{\Gamma(\eta)} \int_0^{\hat{\omega}} d\hat{\omega}' \frac{\hat{S}(\hat{\omega}', \mu_0)}{\mu_0^\eta (\hat{\omega} - \hat{\omega}')^{1-\eta}}, \quad (59)$$

with V_S as given in (54). A similar analytic result for the renormalized shape function was obtained in [16] using a different strategy to solve the evolution equation for the shape function. However, these authors miss a factor 2 in the expression for η , and we disagree with their expression for the function V_S .

From the above equation one can derive scaling relations for the asymptotic behavior of the shape function for $\hat{\omega} \rightarrow 0$ and $\hat{\omega} \rightarrow \infty$ (corresponding to $\omega \rightarrow \bar{\Lambda}$ and $\omega \rightarrow -\infty$). If the function $\hat{S}(\hat{\omega}, \mu_0)$ at the low scale μ_0 vanishes proportional to $\hat{\omega}^\zeta$ near the endpoint, the shape function at a higher scale $\mu_i > \mu_0$ vanishes faster, proportional to $\hat{\omega}^{\zeta+\eta}$. Similarly, if $\hat{S}(\hat{\omega}, \mu_0)$ falls off like $\hat{\omega}^{-\xi}$ for $\hat{\omega} \rightarrow \infty$, the shape function renormalized at a higher scale vanishes like $\hat{\omega}^{-\min(1, \xi)+\eta}$. Irrespective of the initial behavior of the shape function, evolution effects generate a radiative tail that falls off slower than $1/\hat{\omega}$. This fact implies that the normalization integral of $\hat{S}(\hat{\omega}, \mu)$ as well as all positive moments are ultra-violet divergent. The field-theoretic reason is that the bilocal shape-function operator in (9) contains ultra-violet singularities as $z_- \rightarrow 0$, which are not subtracted in the renormalization of the shape function. The situation is analogous to the case of the B -meson light-cone distribution amplitude discussed in [15, 32]. These divergences are never an obstacle in practice. Convolution integrals with the shape function are always cut off at some finite value of $\hat{\omega}$ by virtue of phase-space or some experimental cut.

5 Properties of the shape function

In this section we discuss how moments of the shape function are related with HQET parameters. This will lead us to propose a new, physical scheme for defining a running heavy-quark mass, which is most appropriate for the study of inclusive spectra in the shape-function region. We will also present a model-independent result for the asymptotic behavior of the renormalized shape function (defined in the $\overline{\text{MS}}$ scheme), finding that it is *not* positive definite.

Most of our discussion in this section is phrased in terms of the original (unhatted) shape function $S(\omega, \mu)$. At the end, we formulate the resulting constraints on the function $\hat{S}(\hat{\omega}, \mu)$.

5.1 Shape-function moments in the pole scheme

Naively, ignoring renormalization effects, the moments $M_N = \int_{-\infty}^{\bar{\Lambda}} d\omega \omega^N S(\omega)$ are given by hadronic parameters defined in terms of B -meson matrix elements of local HQET operators [1]. In particular, $M_0 = 1$ fixes the normalization of the shape function, $M_1 = 0$ vanishes by the HQET equation of motion, and $M_2 = -\lambda_1/3$ is determined by the matrix element of the kinetic-energy operator. The vanishing of the first moment is connected with the implicit definition of the heavy-quark pole mass built into the HQET Lagrangian via the equation

of motion $iv \cdot D h = 0$. These moment constraints have been implemented in various model parameterizations for the shape function suggested in the literature [3, 33, 34]. Typically, one makes an ansatz for the shape function depending on a few HQET parameters such as $\bar{\Lambda}$ and λ_1 , and determines the values of these parameters from a fit to experimental data.

Beyond tree level, all moments M_N with $N \geq 0$ receive ultra-violet divergences from the region $\omega \rightarrow -\infty$ (or $\hat{\omega} \rightarrow \infty$). However, as we have mentioned above, the values of ω needed for the description of physical decay rates are always restricted to a finite interval. It is thus sufficient for all purposes to define the moments of the renormalized shape function as

$$M_N(\Lambda_{UV}, \mu) = \int_{-\Lambda_{UV}}^{\bar{\Lambda}} d\omega \omega^N S(\omega, \mu). \quad (60)$$

The dependence of these moments on the renormalization scale μ is controlled by the evolution equation (36). In addition, the moments depend on the lower cutoff on the ω integral. The choice of Λ_{UV} is a matter of convenience, and so we are free to pick a value that is numerically (if not parametrically) large compared with Λ_{QCD} . In this case, as we will now show, the dependence on Λ_{UV} can also be controlled using short-distance methods.

For sufficiently large values of Λ_{UV} it is possible to expand the moments $M_N(\Lambda_{UV}, \mu)$ in a series of B -meson matrix elements of local HQET operators. If for simplicity we set $\Gamma = 1$ in the shape-function operator (which is legitimate, since the Dirac structure is unaltered in HQET), the operators in question are Lorentz-scalar, “leading-twist” operators containing $\bar{h} \dots h$ [1, 2]. These are the operators that mix with $\bar{h}(in \cdot D)^N h$ under renormalization. It is straightforward to find the corresponding operators of a given dimension. The unique dimension-3 operator is $\bar{h}h$. The two operators of dimension 4 are $\bar{h}in \cdot D h$ (class-1) and $\bar{h}iv \cdot D h$ (class-2). The class-2 operator vanishes by the HQET equation of motion. The possible dimension-5 operators are

$$\begin{aligned} \text{class-1:} \quad & \bar{h}(in \cdot D)^2 h, \quad \bar{h}(iD_\perp)^2 h, \\ \text{class-2:} \quad & \bar{h}(iv \cdot D)^2 h, \quad \bar{h}in \cdot D iv \cdot D h, \quad \bar{h}iv \cdot D in \cdot D h, \end{aligned} \quad (61)$$

where again the class-2 operators vanish by the equation of motion. Moreover, it follows from the Feynman rules of HQET that the two class-1 operators do not mix under renormalization, so the operator $\bar{h}(iD_\perp)^2 h$ can be ignored. From dimension 6 on the situation is more complicated, because several class-1 operators exist that can mix with $\bar{h}(in \cdot D)^N h$. For $N = 3$ these are of the form $\bar{h}iD G h$ or $\sum_q \bar{h} \dots q \bar{q} \dots h$, where we omit Lorentz and color indices. We will restrict our discussion to operators of dimension less than 6.

For the operator product expansion of the moments in (60) we need the forward matrix elements

$$\langle O \rangle = \frac{\langle \bar{B}(v) | O | \bar{B}(v) \rangle}{2M_B} \quad (62)$$

of the leading-twist operators between B -meson states in HQET. Using the equation of motion, it can be shown that $\langle \bar{h}h \rangle = 1$, $\langle \bar{h}in \cdot D h \rangle = 0$, and $\langle \bar{h}(in \cdot D)^2 h \rangle = -\lambda_1/3$ [1]. We can thus write an expansion of the form

$$M_N(\Lambda_{UV}, \mu) = \Lambda_{UV}^N \left\{ K_0^{(N)}(\Lambda_{UV}, \mu) + K_2^{(N)}(\Lambda_{UV}, \mu) \cdot \frac{(-\lambda_1)}{3\Lambda_{UV}^2} + O\left[\left(\frac{\Lambda_{QCD}}{\Lambda_{UV}}\right)^3\right] \right\}. \quad (63)$$

This expansion is useful as long as the cutoff Λ_{UV} is chosen much larger than the typical hadronic scale characterizing the matrix elements of the local operators. The matching coefficients $K_n^{(N)}$ in this relation can be calculated using on-shell external b -quark states with residual momentum k . For operators of dimension up to 5 it suffices to calculate two-point functions. (Three and four-point functions would have to be considered at dimension 6.) We first evaluate the moments of the renormalized shape function in (33), finding at one-loop order

$$M_N^{\text{parton}}(\Lambda_{\text{UV}}, \mu) = (n \cdot k)^N \left\{ 1 - \frac{C_F \alpha_s}{\pi} \left(\ln^2 \frac{\Lambda_{\text{UV}} + n \cdot k}{\mu} + \ln \frac{\Lambda_{\text{UV}} + n \cdot k}{\mu} + \frac{\pi^2}{24} \right) - \frac{C_F \alpha_s}{\pi} \sum_{j=1}^N \frac{1}{j} \left(1 + 2 \ln \frac{\Lambda_{\text{UV}} + n \cdot k}{\mu} - \sum_{l=j}^N \frac{2}{l} \right) \left[\left(-\frac{\Lambda_{\text{UV}}}{n \cdot k} \right)^j - 1 \right] \right\}. \quad (64)$$

We then expand this result in powers of $n \cdot k / \Lambda_{\text{UV}}$. Keeping the first three terms in the expansion, we obtain

$$\begin{aligned} M_0^{\text{parton}}(\Lambda_{\text{UV}}, \mu) &= 1 - \frac{C_F \alpha_s}{\pi} \left(\ln^2 \frac{\Lambda_{\text{UV}}}{\mu} + \ln \frac{\Lambda_{\text{UV}}}{\mu} + \frac{\pi^2}{24} \right) \\ &\quad - \frac{C_F \alpha_s}{\pi} \left[\frac{n \cdot k}{\Lambda_{\text{UV}}} \left(2 \ln \frac{\Lambda_{\text{UV}}}{\mu} + 1 \right) + \frac{(n \cdot k)^2}{\Lambda_{\text{UV}}^2} \left(-\ln \frac{\Lambda_{\text{UV}}}{\mu} + \frac{1}{2} \right) + \dots \right], \\ M_1^{\text{parton}}(\Lambda_{\text{UV}}, \mu) &= n \cdot k \left[1 - \frac{C_F \alpha_s}{\pi} \left(\ln^2 \frac{\Lambda_{\text{UV}}}{\mu} - \ln \frac{\Lambda_{\text{UV}}}{\mu} + \frac{\pi^2}{24} - 1 \right) \right] \\ &\quad - \frac{C_F \alpha_s}{\pi} \left[\Lambda_{\text{UV}} \left(-2 \ln \frac{\Lambda_{\text{UV}}}{\mu} + 1 \right) + \frac{(n \cdot k)^2}{\Lambda_{\text{UV}}} 2 \ln \frac{\Lambda_{\text{UV}}}{\mu} + \dots \right], \\ M_2^{\text{parton}}(\Lambda_{\text{UV}}, \mu) &= (n \cdot k)^2 \left[1 - \frac{C_F \alpha_s}{\pi} \left(\ln^2 \frac{\Lambda_{\text{UV}}}{\mu} - 2 \ln \frac{\Lambda_{\text{UV}}}{\mu} + \frac{\pi^2}{24} - \frac{1}{2} \right) \right] \\ &\quad - \frac{C_F \alpha_s}{\pi} \left[\Lambda_{\text{UV}}^2 \ln \frac{\Lambda_{\text{UV}}}{\mu} + n \cdot k \Lambda_{\text{UV}} \left(-2 \ln \frac{\Lambda_{\text{UV}}}{\mu} + 3 \right) + \dots \right]. \end{aligned} \quad (65)$$

In the next step, we calculate the one-loop matrix elements of the local operators $\bar{h} (in \cdot D)^N h$ between heavy-quark states with residual momentum k . The relevant diagrams are the same as in Figure 2, where now the black square represents the local operators. Keeping $v \cdot k$ non-zero to regularize infra-red singularities, we obtain for the bare matrix elements

$$\begin{aligned} \langle \bar{h} (in \cdot D)^N h \rangle &= (n \cdot k)^N \left\{ 1 - \frac{4C_F g_s^2}{(4\pi)^{2-\epsilon}} (-2v \cdot k)^{-2\epsilon} \sum_{j=1}^N \binom{N}{j} \left(\frac{2v \cdot k}{n \cdot k} \right)^j \right. \\ &\quad \left. \times (j-1-\epsilon) \Gamma(j-\epsilon) \Gamma(2\epsilon-j) \right\}. \end{aligned} \quad (66)$$

While the individual diagrams are infra-red divergent, taking the limit $v \cdot k \rightarrow 0$ in the sum of all contributions is possible without encountering singularities. Then the one-loop

contributions vanish, and the matrix elements simply reduce to their tree-level values. In other words, the one-loop contributions correspond to a mixing with class-2 operators, whose hadronic matrix elements vanish by the equations of motions. It follows that in (65) we must identify $(n \cdot k)^n \rightarrow \langle \bar{h} (in \cdot D)^n h \rangle$. Substituting the results for the HQET matrix elements given earlier, we obtain for the Wilson coefficients of the first three moments

$$\begin{aligned} K_0^{(0)} &= 1 - \frac{C_F \alpha_s}{\pi} \left(\ln^2 \frac{\Lambda_{\text{UV}}}{\mu} + \ln \frac{\Lambda_{\text{UV}}}{\mu} + \frac{\pi^2}{24} \right), & K_2^{(0)} &= \frac{C_F \alpha_s}{\pi} \left(\ln \frac{\Lambda_{\text{UV}}}{\mu} - \frac{1}{2} \right), \\ K_0^{(1)} &= \frac{C_F \alpha_s}{\pi} \left(2 \ln \frac{\Lambda_{\text{UV}}}{\mu} - 1 \right), & K_2^{(1)} &= -2 \frac{C_F \alpha_s}{\pi} \ln \frac{\Lambda_{\text{UV}}}{\mu}, \\ K_0^{(2)} &= -\frac{C_F \alpha_s}{\pi} \ln \frac{\Lambda_{\text{UV}}}{\mu}, & K_2^{(2)} &= 1 - \frac{C_F \alpha_s}{\pi} \left(\ln^2 \frac{\Lambda_{\text{UV}}}{\mu} - 2 \ln \frac{\Lambda_{\text{UV}}}{\mu} + \frac{\pi^2}{24} - \frac{1}{2} \right). \end{aligned} \quad (67)$$

At tree level, this reproduces the naive moment relations mentioned at the beginning of this section. Beyond tree level, the moments get corrected by calculable short-distance effects, which can be controlled using fixed-order perturbation theory as long as the ratio Λ_{UV}/μ is of $O(1)$. In particular, the renormalized first moment no longer vanishes, but is proportional to the cutoff Λ_{UV} up to small power corrections.

As mentioned earlier, the value of the first moment is connected with the definition of the heavy-quark mass (see also [26, 28]). The first moment of the renormalized shape function can be made to vanish to all orders in perturbation theory by choosing an appropriate scheme for the definition of m_b . So far our calculations have assumed the definition of the heavy-quark mass as a pole mass, m_b^{pole} , which is implied by the HQET equation of motion $iv \cdot D h = 0$. Results such as (67) are valid in this particular scheme. A more general choice is to allow for a residual mass term δm in HQET, such that $iv \cdot D h = \delta m h$ with $\delta m = O(\Lambda_{\text{QCD}})$ [35]. It is well known that the pole mass is an ill-defined concept, which suffers from infra-red renormalon ambiguities [36, 37]. The parameter $\bar{\Lambda}_{\text{pole}} = M_B - m_b^{\text{pole}}$, which determines the support of the shape function in the pole-mass scheme, inherits the same ambiguities. It is therefore advantageous to eliminate the pole mass in favor of some short-distance mass. For the analysis of inclusive B -meson decays, a proper choice is to use a so-called low-scale subtracted heavy-quark mass $m_b(\mu_f)$ [38], which is obtained from the pole mass by removing a long-distance contribution proportional to a subtraction scale $\mu_f = \text{few} \times \Lambda_{\text{QCD}}$,

$$m_b^{\text{pole}} = m_b(\mu_f) + \mu_f g\left(\alpha_s(\mu), \frac{\mu_f}{\mu}\right) \equiv m_b(\mu_f) + \delta m. \quad (68)$$

As long as $m_b(\mu_f)$ is defined in a physical way, the resulting perturbative expressions after elimination of the pole mass are well-behaved and not plagued by renormalon ambiguities. Replacing the pole mass by the physical mass shifts the values of $n \cdot k$ and ω by an amount δm , since $n \cdot (m_b^{\text{pole}} v + k) = m_b(\mu_f) + (n \cdot k + \delta m)$, and because the covariant derivative in the definition of the shape function in (13) must be replaced by $in \cdot D - \delta m$ [35]. At the same time, $\bar{\Lambda}_{\text{pole}} = \bar{\Lambda}(\mu_f) - \delta m$, where $\bar{\Lambda}(\mu_f) = M_B - m_b(\mu_f)$ is a physical parameter. Note that this leaves the parameter $\hat{\omega} = \bar{\Lambda} - \omega$ and hence the shape function $\hat{S}(\hat{\omega}, \mu)$ invariant. This follows since $\bar{\Lambda}_{\text{pole}} - \omega_{\text{pole}} = \bar{\Lambda}(\mu_f) - (\omega_{\text{pole}} + \delta m)$, where ω_{pole} denotes the value in the pole-mass scheme used so far.

5.2 Shape-function moments in a physical scheme

From now on we will adopt a mass scheme defined by some specific choice of δm . Let us denote by $\omega = \omega_{\text{pole}} + \delta m$ the value of the light-cone momentum variable in that scheme and define “physical” moments M_N^{phys} as in (60), but with all parameters replaced by their values in the new scheme, in particular $\bar{\Lambda} = \bar{\Lambda}(\mu_f)$. Then the expressions for the moments in (64) and (65) change according to the replacements $n \cdot k \rightarrow n \cdot k + \delta m$ and $\Lambda_{\text{UV}} \rightarrow \Lambda_{\text{UV}} - \delta m$ everywhere. We now *choose* δm such that the first moment vanishes, thereby defining a low-scale subtracted heavy-quark mass (with $\mu_f = \Lambda_{\text{UV}}$) to all orders in perturbation theory. We will refer to this mass as the “shape-function mass” m_b^{SF} . This is a “physical”, short-distance mass in the sense that it is free of renormalon ambiguities. (However, the definition of the shape-function mass depends on the renormalization scheme used to define the shape function.) From (65) and (68), it follows that at one-loop order

$$m_b^{\text{pole}} = m_b^{\text{SF}}(\mu_f, \mu) + \mu_f \frac{C_F \alpha_s(\mu)}{\pi} \left[\left(1 - 2 \ln \frac{\mu_f}{\mu} \right) + \frac{2}{3} \frac{(-\lambda_1)}{\mu_f^2} \ln \frac{\mu_f}{\mu} + \dots \right]. \quad (69)$$

Note that after introduction of the shape-function mass the coefficients $K_n^{(1)}$ in the operator-product expansion for the moments in (63) vanish by definition. However, to first order in α_s the values for the coefficients $K_n^{(0)}$ and $K_n^{(2)}$ of the zeroth and second moments given in (67) remain unchanged, since $\delta m = O(\alpha_s)$. This would no longer be true for the coefficients of higher moments.

The shape-function mass can be related to any other short-distance mass using perturbation theory. For instance, at one-loop order its relations to the potential-subtracted mass introduced in [39] and to the kinetic mass defined in [40, 41] read

$$m_b^{\text{SF}}(\mu_f, \mu_f) = m_b^{\text{PS}}(\mu_f) = m_b^{\text{kin}}(\mu_f) + \mu_f \frac{C_F \alpha_s(\mu_f)}{3\pi}. \quad (70)$$

Note that, in addition to the dependence on the subtraction scale μ_f , the shape-function mass depends on the scale μ at which the shape function is renormalized. While it is natural to set $\mu = \mu_f$, as we did here, this is not necessary. Given a value for the shape-function mass for some choice of scales, we can solve (69) to obtain its value for any other choice, using the fact that the pole mass is scale independent.

Proceeding in an analogous way, we can use the second moment to define a physical kinetic-energy parameter, commonly called μ_π^2 . This quantity can be used to replace the HQET parameter λ_1 , which like the pole mass suffers from infra-red renormalon ambiguities [42]. At one-loop order, we obtain

$$\begin{aligned} \frac{\mu_\pi^2(\Lambda_{\text{UV}}, \mu)}{3} &\equiv \frac{M_2^{\text{phys}}(\Lambda_{\text{UV}}, \mu)}{M_0^{\text{phys}}(\Lambda_{\text{UV}}, \mu)} \\ &= -\frac{C_F \alpha_s(\mu)}{\pi} \Lambda_{\text{UV}}^2 \ln \frac{\Lambda_{\text{UV}}}{\mu} + \frac{(-\lambda_1)}{3} \left[1 + \frac{C_F \alpha_s(\mu)}{\pi} \left(3 \ln \frac{\Lambda_{\text{UV}}}{\mu} + \frac{1}{2} \right) \right] + \dots \end{aligned} \quad (71)$$

Taking the ratio of M_2^{phys} and M_0^{phys} has the advantage of eliminating the double logarithmic radiative corrections from this expression. Our definition is similar to the running parameter

μ_π^2 defined in the kinetic scheme [40, 41]. At one-loop order, the two parameters are related by

$$\mu_\pi^2(\mu_f, \mu) = -\mu_f^2 \frac{C_F \alpha_s(\mu_f)}{\pi} + [\mu_\pi^2(\mu_f)]_{\text{kin}} \left[1 + \frac{C_F \alpha_s(\mu_f)}{2\pi} \right]. \quad (72)$$

Given a value for the kinetic energy in the shape-function scheme for some choice of scales, we can solve (71) to obtain its value for any other choice, using that λ_1 is scale independent.

Similarly, each new moment of the renormalized shape function can be used to define a new physical, scale-dependent parameter $A_N(\Lambda_{\text{UV}}, \mu) \equiv M_N^{\text{phys}}(\Lambda_{\text{UV}}, \mu)/M_0^{\text{phys}}(\Lambda_{\text{UV}}, \mu)$, which coincides with the corresponding HQET parameter $A_N = \langle \bar{h} (in \cdot D)^N h \rangle$ at tree level, and which beyond tree level is related to HQET parameters through well-controlled perturbative expressions. Obviously, the presence of power divergences implies that higher moments are progressively less sensitive to HQET parameters, since they are dominated by the perturbative terms of order $\alpha_s \Lambda_{\text{UV}}^N$.

5.3 Moments of the scheme-independent function $\hat{S}(\hat{\omega}, \mu)$

It will be useful to rewrite the moment relations derived above in terms of the variable $\hat{\omega} = \bar{\Lambda} - \omega$, which is invariant under redefinitions of the heavy-quark mass. Defining a new set of scheme-independent moments

$$\hat{M}_N(\mu_f, \mu) = \int_0^{\mu_f + \bar{\Lambda}(\mu_f, \mu)} d\hat{\omega} \hat{\omega}^N \hat{S}(\hat{\omega}, \mu), \quad (73)$$

we obtain

$$\begin{aligned} \hat{M}_0(\mu_f, \mu) &= 1 - \frac{C_F \alpha_s(\mu)}{\pi} \left(\ln^2 \frac{\mu_f}{\mu} + \ln \frac{\mu_f}{\mu} + \frac{\pi^2}{24} \right) + \frac{C_F \alpha_s(\mu)}{\pi} \left(\ln \frac{\mu_f}{\mu} - \frac{1}{2} \right) \frac{\mu_\pi^2(\mu_f, \mu)}{3\mu_f^2} + \dots, \\ \frac{\hat{M}_1(\mu_f, \mu)}{\hat{M}_0(\mu_f, \mu)} &= \bar{\Lambda}(\mu_f, \mu), \quad \frac{\hat{M}_2(\mu_f, \mu)}{\hat{M}_0(\mu_f, \mu)} = \frac{\mu_\pi^2(\mu_f, \mu)}{3} + \bar{\Lambda}(\mu_f, \mu)^2, \end{aligned} \quad (74)$$

where the parameters $\bar{\Lambda}(\mu_f, \mu) = M_B - m_b^{\text{SF}}(\mu_f, \mu)$ and $\mu_\pi^2(\mu_f, \mu)$ should be considered as known physical quantities. Using the relations in the previous subsection, we have

$$\begin{aligned} m_b^{\text{SF}}(\mu_f, \mu) &= m_b^{\text{SF}}(\mu_*, \mu_*) + \mu_* \frac{C_F \alpha_s(\mu_*)}{\pi} \\ &\quad - \mu_f \frac{C_F \alpha_s(\mu)}{\pi} \left[\left(1 - 2 \ln \frac{\mu_f}{\mu} \right) + \frac{2}{3} \frac{\mu_\pi^2(\mu_f, \mu)}{\mu_f^2} \ln \frac{\mu_f}{\mu} \right], \\ \mu_\pi^2(\mu_f, \mu) &= \mu_\pi^2(\mu_*, \mu_*) \left[1 - \frac{C_F \alpha_s(\mu_*)}{2\pi} + \frac{C_F \alpha_s(\mu)}{\pi} \left(3 \ln \frac{\mu_f}{\mu} + \frac{1}{2} \right) \right] - 3\mu_f^2 \frac{C_F \alpha_s(\mu)}{\pi} \ln \frac{\mu_f}{\mu}, \end{aligned} \quad (75)$$

where μ_* denotes the scale at which initial values for the two parameters are obtained, for instance using relations such as (70) and (72). These relations are particularly simple if one chooses $\mu_f = \mu$.

In the relations above we have eliminated the unphysical HQET parameter λ_1 in favor of the physical parameter μ_π^2 defined in the shape-function scheme. At first sight, this seems to threaten the convergence of the operator product expansion. For instance, the term proportional to μ_π^2 in the expression for the zeroth moment \hat{M}_0 in (74) contains a *leading-power* perturbative contribution of order $\alpha_s^2(\mu)$, and similar contributions would arise from all other terms in the expansion. These contributions would have to be subtracted from the Wilson coefficient of the first term, if this coefficient were computed to two-loop order. The overall convergence of the operator product expansion is unaffected by this reorganization of perturbative corrections.

5.4 Asymptotic behavior of the shape function

The fact that for sufficiently large values of the cutoff the moments of the shape function can be calculated using an operator-product expansion implies that a similar expansion can be used to obtain a model-independent description of the asymptotic behavior of the shape function. Taking the derivative of the zeroth moment \hat{M}_0 in (73) with respect to μ_f , one obtains

$$\hat{S}(\hat{\omega}, \mu) \Big|_{\hat{\omega}=\mu_f+\bar{\Lambda}(\mu_f, \mu)} = \left(1 - \frac{dm_b^{\text{SF}}(\mu_f, \mu)}{d\mu_f}\right)^{-1} \frac{d}{d\mu_f} \hat{M}_0(\mu_f, \mu). \quad (76)$$

This relation can be trusted as long as $\mu_f \gg \Lambda_{\text{QCD}}$. It allows us to determine the behavior of the shape function for large values of $\hat{\omega}$. From (74) we find at one-loop order

$$\hat{S}(\hat{\omega}, \mu) = -\frac{C_F \alpha_s(\mu)}{\pi} \frac{1}{\hat{\omega} - \bar{\Lambda}} \left[\left(2 \ln \frac{\hat{\omega} - \bar{\Lambda}}{\mu} + 1\right) + \frac{2}{3} \frac{\mu_\pi^2}{(\hat{\omega} - \bar{\Lambda})^2} \left(\ln \frac{\hat{\omega} - \bar{\Lambda}}{\mu} - 1\right) + \dots \right]. \quad (77)$$

The precise definitions of $\bar{\Lambda}$ and μ_π^2 are not specified at this order. (Note that the shape function cannot depend on the value of the cutoff μ_f .) We have checked that this asymptotic behavior of the shape function is consistent with the evolution equation (59) when expanded to first order in α_s .

Relation (77) is a model-independent result as long as $\hat{\omega} \gg \Lambda_{\text{QCD}}$. We stress the remarkable fact that this radiative tail of the shape function is *negative*, in contrast with the naive expectation based on a probabilistic interpretation of the shape function as a momentum distribution function. The point is that the definition of the renormalized shape function requires scheme-dependent ultra-violet subtractions. From (77) it follows that the shape function must have a zero, which for sufficiently large μ is located at a value $\hat{\omega}_0 \approx \bar{\Lambda} + \mu/\sqrt{e}$.

6 Recapitulation

We have now completed the conceptual part of this paper. Before turning to phenomenological applications, let us briefly summarize the discussion so far. The hadronic physics governing the inclusive semileptonic decay $\bar{B} \rightarrow X_u l^- \bar{\nu}$ is encoded in the structure functions W_i appearing in the Lorentz decomposition of the hadronic tensor $W^{\mu\nu}$ in (17). In the shape-function region, only two combinations of these functions are required at leading order in Λ_{QCD}/m_b . They

follow from the factorization formula (14) using the explicit results for the hard functions H_{ij} and the jet function J derived in this paper. Explicitly, we obtain at next-to-leading order in renormalization-group improved perturbation theory

$$\begin{aligned} \frac{W_1}{2} &= \left\{ 1 + \frac{C_F \alpha_s(m_b)}{4\pi} \left[-4 \ln^2 y + (6 - c) \ln y - \frac{2 \ln y}{1 - y} - 4L_2(1 - y) - \frac{\pi^2}{6} - 12 \right] \right\} \\ &\quad \times y^{-1-a} e^{V_H(m_b, \mu_i)} \int_0^{n \cdot P_H} d\hat{\omega} \hat{J}(\hat{p}_\omega^2, y, \mu_i) \hat{S}(\hat{\omega}, \mu_i) + \dots, \\ \frac{W_4}{2} + \frac{m_b W_5}{4} &= \frac{C_F \alpha_s(m_b)}{4\pi} \frac{2 \ln y}{1 - y} y^{-1-a} e^{V_H(m_b, \mu_i)} \int_0^{n \cdot P_H} d\hat{\omega} \hat{J}(\hat{p}_\omega^2, y, \mu_i) \hat{S}(\hat{\omega}, \mu_i) + \dots, \end{aligned} \quad (78)$$

where the dots represent power corrections in Λ_{QCD}/m_b . In these expressions $y = \bar{n} \cdot p/m_b$ is a partonic scaling variable, while $\hat{p}_\omega^2 = m_b(n \cdot P_H - \hat{\omega})$ depends on the hadronic variable $n \cdot P_H = E_H - |\vec{P}_H|$. In all our results, m_b denotes the heavy-quark mass defined in the “shape-function scheme” introduced in Section 5 (see also Section 9 below). The jet function $\hat{J}(\hat{p}_\omega^2, y, \mu_i)$ at an intermediate hard-collinear scale $\mu_i \sim \sqrt{m_b \Lambda_{\text{QCD}}}$ can be calculated in fixed-order perturbation theory. The relevant expression valid at one-loop order is given in (27). The above results contain a variety of renormalization-group functions, which arise in the solution of evolution equations discussed in Section 4. The explicit form of the Sudakov exponent V_H can be found in (42). This function is independent of the kinematic variables y and \hat{p}_ω^2 . In addition, we need

$$\begin{aligned} a &= \frac{\Gamma_0}{\beta_0} \ln r_1 = \frac{16}{25} \ln \frac{\alpha_s(\mu_i)}{\alpha_s(m_b)}, \\ c &= \frac{4}{\beta_0} \left(\frac{\Gamma_1}{\Gamma_0} - \frac{\beta_1}{\beta_0} \right) (r_1 - 1) = \left(\frac{10556}{1875} - \frac{12\pi^2}{25} \right) \left(\frac{\alpha_s(\mu_i)}{\alpha_s(m_b)} - 1 \right). \end{aligned} \quad (79)$$

For simplicity, we have identified the high-energy matching scale μ_h introduced in Section 4 with the heavy-quark mass m_b . Our results are formally independent of the precise choice of $\mu_h \sim m_b$. The numerical effect of the residual μ_h dependence remaining after truncation of the perturbative expansion has been studied in [29] and was found to be small.

The function $\hat{S}(\hat{\omega}, \mu_i)$ in (78) is the shape function after the transformation of variables from ω to $\hat{\omega} = \bar{\Lambda} - \omega$. The limits of integration for the variable $\hat{\omega}$ (i.e., $0 \leq \hat{\omega} \leq n \cdot P_H$) are set by hadronic kinematics and are independent of the definition of the heavy-quark mass. The shape function is a non-perturbative object, which at present cannot be predicted from first principles. It enters our results (78) renormalized at the intermediate hard-collinear scale μ_i . In (59), we have presented an analytic formula (valid at leading order in renormalization-group improved perturbation theory) that relates the shape function at a high scale to the shape function renormalized at a low hadronic scale. Many properties of the shape function that were so far unknown have been derived in Section 5. In particular, we have given explicit formulae relating the moments of the shape function to HQET parameters, and we have proved that the shape function has a negative tail for large values of $\hat{\omega}$, whose explicit form can be calculated using an operator product expansion. These new insights about the shape function

will be very helpful in constructing a realistic model for the function $\hat{S}(\hat{\omega}, \mu_i)$, which can then be refined by tuning it to experimental data such as the photon energy spectrum in inclusive $\bar{B} \rightarrow X_s \gamma$ decays.

7 Differential decay rates and spectra

In the shape-function region considered in this work, the hadronic tensor is most naturally expressed in terms of the variables $n \cdot P_H$ and $\bar{n} \cdot p$, where $p = m_b v - q = P_H - \bar{\Lambda} v$ is the momentum of the final-state hadronic jet in the parton picture. This would remain true if we worked to higher order in the collinear expansion. It is thus useful to derive expressions for the decay rates in terms of these variables. Our theoretical results are valid as long as $n \cdot P_H$ can be considered as being of order a hadronic scale (say, a few $\times \Lambda_{\text{QCD}}$), whereas $\bar{n} \cdot p$ is integrated over a domain of order $m_b \gg \Lambda_{\text{QCD}}$. It is this integration which provides a sampling over sufficiently many hadronic final states needed to ensure quark-hadron duality. The duality hypothesis underlies any description of inclusive decay rates using short-distance methods [43].

Under these conditions, it is appropriate to describe the distribution in $\bar{n} \cdot p$ in terms of a *partonic* scaling variable $y = \bar{n} \cdot p / m_b$, while the distribution in the orthogonal light-cone component is described in terms of the dimensionful *hadronic* variable $P_+ \equiv n \cdot P_H = E_H - |\vec{P}_H|$. At leading order in Λ_{QCD}/m_b , we obtain from [18] the triple differential decay rate

$$\frac{d^3\Gamma}{d\bar{x} dy dP_+} = 12m_b \Gamma_{\text{tree}} y(y - \bar{x}) \left[(1 + \bar{x} - y) \frac{W_1}{2} + \bar{x} \left(\frac{W_4}{2} + \frac{m_b W_5}{4} \right) \right] + \dots, \quad (80)$$

where $\bar{x} = 1 - x$, and $x = 2E_l/m_b$ is a scaling variable proportional to the energy of the charged lepton measured in the B -meson rest frame. $\Gamma_{\text{tree}} = G_F^2 |V_{ub}|^2 (m_b^{\text{pole}})^5 / (192\pi^3)$ denotes the tree-level expression for the total $\bar{B} \rightarrow X_u l^- \bar{\nu}$ decay rate obtained at leading order in the heavy-quark expansion. Phase space is such that

$$0 \leq P_+ \leq M_B - 2E_l = m_b \bar{x} + \bar{\Lambda}, \quad \frac{P_+ - \bar{\Lambda}}{m_b} \leq \bar{x} \leq y \leq 1. \quad (81)$$

The structure functions W_i have support only for $y > 0$, see (27). If the lepton scaling variable \bar{x} is integrated over a domain of order unity (meaning that E_l is integrated over a domain of order $m_b \gg \Lambda_{\text{QCD}}$), one can replace the second condition by $0 \leq \bar{x} \leq y \leq 1$ at leading power in Λ_{QCD}/m_b . If, on the other hand, the lepton energy is restricted to be close to its kinematic limit, $E_l \approx M_B/2$, then $\bar{x} = O(\Lambda_{\text{QCD}}/m_b)$, and at leading order the rate (80) can be simplified to

$$\frac{d^3\Gamma}{dE_l dy dP_+} = 24\Gamma_{\text{tree}} y^2 (1 - y) \frac{W_1}{2} + \dots, \quad (82)$$

with $0 \leq y \leq 1$ and $0 \leq P_+ \leq M_B - 2E_l$.

It will be useful to develop some intuition for the light-cone momentum variables. In general, the hadronic tensor can be described in terms of the quantities

$$P_+ = E_H - |\vec{P}_H|, \quad P_- = E_H + |\vec{P}_H|, \quad (83)$$

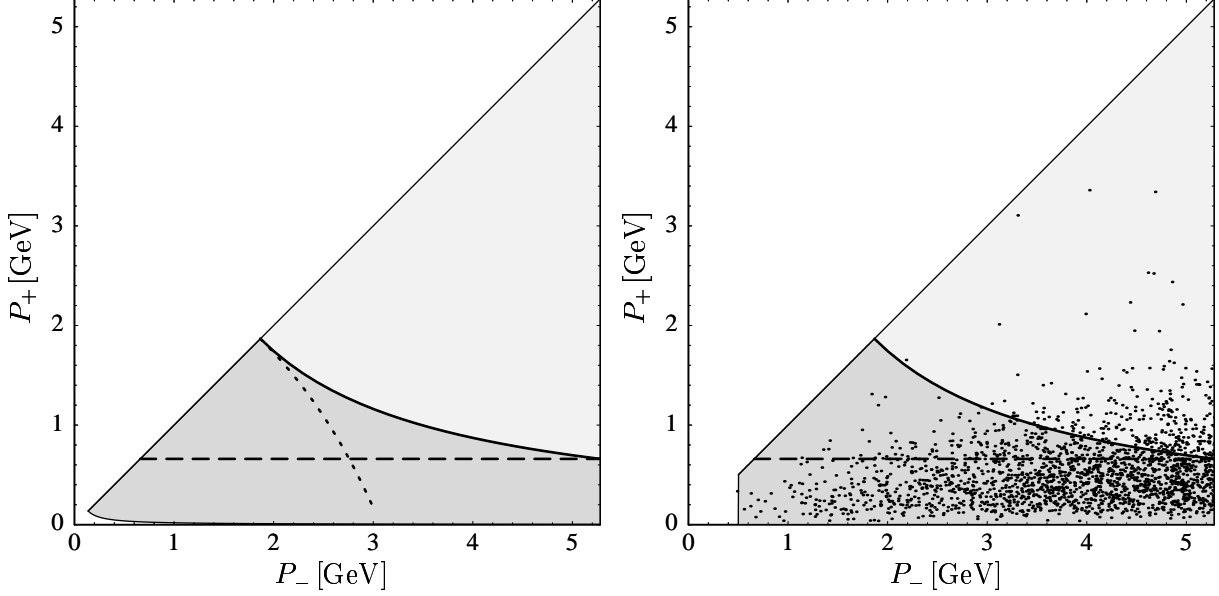


Figure 3: Hadronic phase space for the light-cone variables P_- and P_+ (left), and theory phase space for $m_b = 4.8$ GeV (right). The scatter points indicate the distribution of events as predicted by the model of [18]. In each plot the solid line separates the regions where $s_H < M_D^2$ (dark gray) and $s_H > M_D^2$ (light gray), whereas the dashed line corresponds to $P_+ = M_D^2/M_B$. The dotted line in the first plot shows the contour where $q^2 = (M_B - M_D)^2$.

whose true phase-space is $M_\pi^2/P_- \leq P_+ \leq P_- \leq M_B$, corresponding to a triangular region in the (P_-, P_+) plane with a tiny portion near the P_- axis left unpopulated. The variable P_- is related to our parton variables by $P_- = \bar{n} \cdot p + \bar{\Lambda} = m_b y + \bar{\Lambda}$. In our theoretical description based on quark-hadron duality P_+ starts from 0, while the small region with $P_- < \bar{\Lambda}$ is left unpopulated. This is illustrated in Figure 3. Contours of constant hadronic or leptonic invariant mass in the (P_-, P_+) plane are easy to visualize, since

$$s_H = P_H^2 = P_+ P_-, \quad q^2 = (M_B - P_+)(M_B - P_-) \quad (84)$$

are given by simple expressions. The solid and dotted lines in the left-hand plot in Figure 3 show the contours where $s_H = M_D^2$ and $q^2 = (M_B - M_D)^2$, respectively, which can be used to separate $\bar{B} \rightarrow X_u l^- \bar{\nu}$ events from semileptonic decays with charm hadrons in the final state. The dashed horizontal line shows the maximum allowed value of P_+ when a cut $E_l \geq (M_B^2 - M_D^2)/(2M_B)$ is applied to the charged-lepton energy, which implies $P_+ \leq M_D^2/M_B$. This cut is another way of eliminating the charm background. In the right-hand plot, we indicate the density of events in theory phase space obtained using the model of [18].¹ The

¹While not rigorously implementing shape-function effects beyond tree level, the model of [18] has the advantage that it interpolates between the shape-function region and the remainder of phase space, where a local operator product expansion can be employed. On the contrary, our more rigorous discussion here is limited to the region of hard-collinear jet momenta. We believe that the scatter plot shown in the figure provides a reasonably realistic impression of the population in phase space.

vast majority of events is located in the shape-function region of small P_+ and large P_- .

In the remainder of this section, we present exact analytic results, valid at leading order in Λ_{QCD}/m_b and at next-to-leading order in renormalization-group improved perturbation theory, for a variety of spectra in $\bar{B} \rightarrow X_u l^- \bar{\nu}$ decays. They are obtained by using our results (78) in conjunction with the expressions for the differential rates in (80) or (82), as appropriate. Our strategy will always be to integrate over the scaling variable y before integrating over the hadronic variable P_+ , changing variables from P_+ to $\hat{p}_\omega^2 = m_b(P_+ - \hat{\omega})$. In this step, one must carefully evaluate the effect of the star distributions contained in the jet function $\hat{J}(\hat{p}_\omega^2, y, \mu_i)$, using the definitions in (19). The integral over the shape-function variable $\hat{\omega}$ is left until the end, so that our formulae can be evaluated once an explicit form for the shape function is assumed. We will always present fractional decay rates normalized to the total inclusive rate

$$\Gamma(\bar{B} \rightarrow X_u l^- \bar{\nu}) \equiv \Gamma_{\text{tot}} = \Gamma_{\text{tree}} \left[1 + \frac{C_F \alpha_s(m_b)}{4\pi} \left(\frac{25}{2} - 2\pi^2 \right) \right] + \dots, \quad (85)$$

where the dots represent higher-order perturbative corrections as well as power corrections of order $(\Lambda_{\text{QCD}}/m_b)^2$ and higher. This procedure offers the advantage of eliminating the strong sensitivity to the heavy-quark (pole) mass. Replacing Γ_{tree} by Γ_{tot} adds a contribution $(2\pi^2 - \frac{25}{2})$ to the coefficient of the hard correction to the function W_1 in (78). Our predictions for normalized rate fractions can be turned into predictions for absolute rates with the help of an independent theoretical prediction for the total $\bar{B} \rightarrow X_u l^- \bar{\nu}$ rate obtained using a local operator product expansion.

The integrals over the parton variable y encountered in our analysis can be reduced to a set of master integrals defined as

$$\begin{aligned} I_1(b, z) &= \int_0^z dy y^b = \frac{z^{1+b}}{1+b}, \\ I_2(b, z) &= \int_0^z dy y^b \ln y = \frac{z^{1+b}}{1+b} \left(\ln z - \frac{1}{1+b} \right), \\ I_3(b, z) &= \int_0^z dy y^b \ln^2 y = \frac{z^{1+b}}{1+b} \left(\ln^2 z - \frac{2 \ln z}{1+b} + \frac{2}{(1+b)^2} \right), \\ I_4(b, z) &= \int_0^z dy y^b \frac{\ln y}{1-y} = \sum_{j=0}^{\infty} \frac{z^{1+b+j}}{1+b+j} \left(\ln z - \frac{1}{1+b+j} \right), \\ I_5(b, z) &= \int_0^z dy y^b L_2(1-y) = \frac{z^{1+b}}{1+b} L_2(1-z) - \frac{I_4(1+b, z)}{1+b}, \end{aligned} \quad (86)$$

where $b > -1$ and $z \leq 1$ are arbitrary real numbers. The integral I_4 can be expressed in terms of the incomplete β function $B(z, a, b)$ and the Lerch transcendent $\Phi(z, a, b)$ as

$$I_4(b, z) = \ln z B(z, 1+b, 0) - z^{1+b} \Phi(z, 2, 1+b). \quad (87)$$

We note the useful relations

$$I_4(1+b, z) = I_4(b, z) - I_2(b, z), \quad I_4(b, 1) = -\psi'(1+b), \quad (88)$$

where $\psi'(z)$ is the derivative of the Euler ψ function.

7.1 Charged-lepton energy spectrum

As a first application, we study the distribution of the charged-lepton energy near the kinematic endpoint. Specifically, we assume that $M_B - 2E_l$ is of order a hadronic scale. Starting from the triple differential rate in (82), we obtain for the normalized energy spectrum

$$\begin{aligned} \frac{1}{\Gamma_{\text{tot}}} \frac{d\Gamma}{dE_l} = & \frac{4T(a)}{m_b} e^{V_H(m_b, \mu_i)} \int_0^{M_B - 2E_l} d\hat{\omega} \hat{S}(\hat{\omega}, \mu_i) \left\{ 1 + \frac{C_F \alpha_s(m_b)}{4\pi} H(a) \right. \\ & + \frac{C_F \alpha_s(\mu_i)}{4\pi} \left[2 \ln^2 \frac{m_b(M_B - 2E_l - \hat{\omega})}{\mu_i^2} + (4f_2(a) - 3) \ln \frac{m_b(M_B - 2E_l - \hat{\omega})}{\mu_i^2} \right. \\ & \left. \left. + (7 - \pi^2 - 3f_2(a) + 2f_3(a)) \right] \right\}. \end{aligned} \quad (89)$$

Here

$$\begin{aligned} T(a) &= 6 \left[I_1(1 - a, 1) - I_1(2 - a, 1) \right], \\ f_n(a) &= \frac{I_n(1 - a, 1) - I_n(2 - a, 1)}{I_1(1 - a, 1) - I_1(2 - a, 1)}, \\ H(a) &= \frac{11\pi^2}{6} - \frac{49}{2} + (6 - c)f_2(a) - 4f_3(a) - 2f_4(a) - 4f_5(a). \end{aligned} \quad (90)$$

Using the results for the master integrals in (86), one readily derives the explicit formulae

$$\begin{aligned} T(a) &= \frac{6}{(3 - a)(2 - a)}, \\ H(a) &= \frac{11\pi^2}{6} - \frac{45}{2} - \frac{2(146 - 162a + 59a^2 - 7a^3)}{(3 - a)^2(2 - a)^2} - 4\psi'(2 - a) - c f_2(a), \\ f_2(a) &= -\frac{5 - 2a}{(3 - a)(2 - a)}, \quad f_3(a) = \frac{2(19 - 15a + 3a^2)}{(3 - a)^2(2 - a)^2}. \end{aligned} \quad (91)$$

At leading power in Λ_{QCD}/m_b the heavy-quark mass in the denominator of the prefactor on the right-hand side of (89) can be replaced by $m_b + \omega = M_B - \hat{\omega}$, which removes any sensitivity to the definition of m_b . This replacement can indeed be justified by studying power corrections to the shape function [44, 45].

All our results for decay rates will have a similar structure, but the definitions of the functions T , f_n , and H will be different in each case. The product $T e^{V_H}$ resums the leading double and single-logarithmic corrections to all orders in perturbation theory. The tree-level result can be recovered by setting $V_H = 0$ and $a = 0$, in which case $T(0) = 1$, and the spectrum is simply given in terms of an integral over the shape function [1]. The next-to-leading order terms can be divided into an $\hat{\omega}$ -independent hard function $H(a)$, whose structure follows from the form of the hard corrections in (78), and a sum of hard-collinear radiative corrections, which follow from the integration over the jet function.

Using the above result, it is straightforward to calculate the fraction $F_E = \Gamma(E_l \geq E_0)/\Gamma_{\text{tot}}$ of all $\bar{B} \rightarrow X_u l^- \bar{\nu}$ events with charged-lepton energy above a threshold E_0 . Defining $\Delta_E = M_B - 2E_0$, we find

$$F_E(\Delta_E) = T(a) e^{V_H(m_b, \mu_i)} \int_0^{\Delta_E} d\hat{\omega} \frac{2(\Delta_E - \hat{\omega})}{M_B - \hat{\omega}} \hat{S}(\hat{\omega}, \mu_i) \left\{ 1 + \frac{C_F \alpha_s(m_b)}{4\pi} H(a) \right. \\ \left. + \frac{C_F \alpha_s(\mu_i)}{4\pi} \left[2 \ln^2 \frac{m_b(\Delta_E - \hat{\omega})}{\mu_i^2} + (4f_2(a) - 7) \ln \frac{m_b(\Delta_E - \hat{\omega})}{\mu_i^2} \right. \right. \\ \left. \left. + (14 - \pi^2 - 7f_2(a) + 2f_3(a)) \right] \right\}. \quad (92)$$

The fraction $F_E(\Delta_E)$ is given in terms of a weighted integral over the shape function, with a weight factor of order Λ_{QCD}/m_b that vanishes at the upper end of integration. As a result, only a small fraction of events is contained in the lepton endpoint region.

7.2 Hadronic P_+ spectrum

A cut on the charged-lepton energy restricts the variable P_+ to be less than Δ_E . On the contrary, however, a cut on P_+ does *not* restrict the lepton energy to be in the endpoint region. In fact, according to (81) the integration over \bar{x} can be taken to run from 0 to 1 at leading power if P_+ is small. It follows that the fraction of events with $P_+ \leq \Delta_E$ samples the same hadronic phase space as the lepton-endpoint cut, but it contains significantly more events. Such a cut therefore offers an excellent opportunity to determine the CKM matrix element $|V_{ub}|$.

The calculation of the fraction $F_P(\Delta_P) = \Gamma(P_+ \leq \Delta_P)/\Gamma_{\text{tot}}$ of all $\bar{B} \rightarrow X_u l^- \bar{\nu}$ events with hadronic light-cone momentum P_+ below a threshold Δ_P starts from the expression for the triple differential rate in (80). We integrate over \bar{x} and y in the range $0 \leq \bar{x} \leq y \leq 1$ before integrating over P_+ . The result is

$$F_P(\Delta_P) = T(a) e^{V_H(m_b, \mu_i)} \int_0^{\Delta_P} d\hat{\omega} \hat{S}(\hat{\omega}, \mu_i) \left\{ 1 + \frac{C_F \alpha_s(m_b)}{4\pi} H(a) \right. \\ \left. + \frac{C_F \alpha_s(\mu_i)}{4\pi} \left[2 \ln^2 \frac{m_b(\Delta_P - \hat{\omega})}{\mu_i^2} + (4f_2(a) - 3) \ln \frac{m_b(\Delta_P - \hat{\omega})}{\mu_i^2} \right. \right. \\ \left. \left. + (7 - \pi^2 - 3f_2(a) + 2f_3(a)) \right] \right\}, \quad (93)$$

where now

$$T(a) = 6I_1(2 - a, 1) - 4I_1(3 - a, 1), \\ H(a) = \frac{11\pi^2}{6} - \frac{49}{2} + (6 - c)f_2(a) - 4f_3(a) - 2[f_4(a) - \Delta f_4(a)] - 4f_5(a), \quad (94)$$

and

$$\begin{aligned} f_n(a) &= \frac{3I_n(2-a, 1) - 2I_n(3-a, 1)}{3I_1(2-a, 1) - 2I_1(3-a, 1)}, \\ \Delta f_4(a) &= \frac{I_4(3-a, 1)}{3I_1(2-a, 1) - 2I_1(3-a, 1)}. \end{aligned} \quad (95)$$

The contribution Δf_4 arises from the terms contained in the structure functions W_4 and W_5 in (78). Using the analytic results for the master integrals yields

$$\begin{aligned} T(a) &= \frac{2(6-a)}{(4-a)(3-a)}, \\ H(a) &= \frac{11\pi^2}{6} - \frac{49}{2} - \frac{4(486 - 389a + 103a^2 - 9a^3)}{(6-a)(4-a)^2(3-a)^2} - 4\psi'(3-a) - c f_2(a), \\ f_2(a) &= -\frac{30 - 12a + a^2}{(6-a)(4-a)(3-a)}, \quad f_3(a) = \frac{2(138 - 90a + 18a^2 - a^3)}{(6-a)(4-a)^2(3-a)^2}. \end{aligned} \quad (96)$$

Comparing the result for $F_P(\Delta_P)$ in (93) with the expression for $F_E(\Delta_E)$ in (92) we observe that, as anticipated, the cut on hadronic P_+ contains a much larger fraction of all $\bar{B} \rightarrow X_u l^- \bar{\nu}$ events. In fact, $F_P(\Delta_P)$ is directly given in terms of an integral over the shape function, without a weight function of order Λ_{QCD}/m_b . If we neglect radiative corrections for a moment, we simply have $F_P(\Delta_P) = \int_0^{\Delta_P} d\hat{\omega} \hat{S}(\hat{\omega})$, where the shape function is expected to peak at a position $\hat{\omega} \approx \bar{\Lambda} \approx 0.5 \text{ GeV}$. For the “optimal cut” $P_+ \leq M_D^2/M_B \simeq 0.66 \text{ GeV}$, which eliminates the charm background entirely, we thus expect that more than half of all events are contained in the event fraction $F_P(\Delta_P)$. The hadronic P_+ spectrum therefore offers a very promising new avenue for a high-precision measurement of $|V_{ub}|$.

In a realistic measurement, it is often necessary to implement a loose cut on the lepton energy in order to eliminate soft leptons, which can be difficult to measure in the detector. Let us discuss how our results would change in the presence of such a cut. Assume that we require $E_l \geq E_0$ with E_0 of order 1 GeV or so, corresponding to $\bar{x} \leq \bar{x}_0 = 1 - 2E_0/m_b$ with $\bar{x}_0 = O(1)$. Our expression for the event fraction $F_P(\Delta_P)$ in (93) remains valid, except that the master functions now become functions of the parameter \bar{x}_0 . We find that $T(a)$, $f_n(a)$ and $\Delta f_4(a)$ in (94) and (95) get replaced by

$$\begin{aligned} T(a, \bar{x}_0) &= 2\bar{x}_0^2(3 + 2\bar{x}_0) \left[I_1(-a, \bar{x}_0) - I_1(-a, 1) \right] - 12\bar{x}_0(1 + \bar{x}_0) \left[I_1(1-a, \bar{x}_0) - I_1(1-a, 1) \right] \\ &\quad + 12\bar{x}_0 \left[I_1(2-a, \bar{x}_0) - I_1(2-a, 1) \right] + 6I_1(2-a, \bar{x}_0) - 4I_1(3-a, \bar{x}_0), \\ f_n(a, \bar{x}_0) &= \frac{[\text{expression for } T(a, \bar{x}_0) \text{ with } I_1 \rightarrow I_n]}{T(a, \bar{x}_0)}, \\ \Delta f_4(a, \bar{x}_0) &= \frac{4\bar{x}_0^3 \left[I_4(-a, \bar{x}_0) - I_4(-a, 1) \right] - 6\bar{x}_0^2 \left[I_4(1-a, \bar{x}_0) - I_4(1-a, 1) \right] + 2I_4(3-a, \bar{x}_0)}{T(a, \bar{x}_0)}. \end{aligned} \quad (97)$$

For $\bar{x}_0 = 1$ these complicated results reduce to the simpler expressions given above. Numerically, the cut on the lepton energy has a minor effect provided that \bar{x}_0 is larger than about 0.6, corresponding to a lower cutoff E_0 less than about 1 GeV.

7.3 Hadronic invariant mass spectrum

A cut $\sqrt{s_H} \leq M_D$ on the hadronic invariant mass in the final state constitutes the ideal separator between $\bar{B} \rightarrow X_u l^- \bar{\nu}$ and $\bar{B} \rightarrow X_c l^- \bar{\nu}$ events, since any final state containing a charm hadron has invariant mass above M_D . The left-hand plot in Figure 3 shows that such a cut fully contains the region with $P_+ \leq M_D^2/M_B$ considered earlier. In addition, the hadronic invariant mass cut contains a triangle-shaped region of larger P_+ , which culminates in a cusp where $P_+ = P_- = M_D$. Near the cusp, both light-cone momentum components are of the same order, and hence this portion of phase space lies outside the shape-function region. In other words, the region near the cusp is a dangerous one (a “Bermuda triangle”), where the theoretical description based on the collinear expansion breaks down. A priori, then, it is not evident that we can compute the fractional rate $F_M(s_0) = \Gamma(s_H \leq s_0)/\Gamma_{\text{tot}}$ in a controlled heavy-quark expansion.

To see what happens, it is instructive to first ignore radiative corrections. At tree level, it is straightforward to obtain

$$F_M(s_0) = \int_0^{\Delta_s} d\hat{\omega} \hat{S}(\hat{\omega}) + \int_{\Delta_s}^{\sqrt{s_0}} d\hat{\omega} \hat{S}(\hat{\omega}) \left(\frac{\Delta_s}{\hat{\omega}} \right)^3 \left(2 - \frac{\Delta_s}{\hat{\omega}} \right), \quad (98)$$

where $\Delta_s = s_0/M_B$. The calculation of this event fraction requires knowledge of the shape function over a wider range in $\hat{\omega}$ than in the case of the event fraction with a cut on P_+ . It is therefore more difficult to extract the relevant hadronic information from the $\bar{B} \rightarrow X_s \gamma$ photon spectrum. The first integral is the same as in (93) and corresponds to the region in phase space where $P_+ \leq s_0/M_B$. Note that the ratio $\Delta_s = s_0/M_B$ plays the same role as the cutoff Δ_P on the P_+ spectrum. The second integral corresponds to the phase space above the dashed line in Figure 3. The region near the cusp corresponds to the upper integration region in the second integral. Note that, due to the rapid fall-off of the integrand, the “Bermuda triangle” only gives a power-suppressed contribution to the decay rate and so can be ignored at leading order in the heavy-quark expansion. We will address this point in more detail below.

When radiative corrections are included, the result for the integrated hadronic invariant mass spectrum becomes rather complicated. It is convenient to split up the integration region in phase space into a box-shaped region with $P_+ \leq s_0/M_B$ and a triangular shaped region with $s_0/M_B < P_+ \leq \sqrt{s_0}$. Writing

$$F_M(s_0) = F_M^{\text{box}}(s_0) + F_M^{\text{triangle}}(s_0), \quad \text{with} \quad F_M^{\text{box}}(s_0) = F_P(\Delta_s), \quad (99)$$

we find that the box contribution is given by the expression for the rate fraction $F_P(\Delta_P)$ in (93) evaluated with $\Delta_P = \Delta_s = s_0/M_B$. For the remaining contribution from the triangular

region, we obtain

$$F_M^{\text{triangle}}(s_0) = e^{V_H(m_b, \mu_i)} \int_{\Delta_s}^{\sqrt{s_0}} d\hat{\omega} \hat{S}(\hat{\omega}, \mu_i) \left[G_1(\Delta_s/\hat{\omega}) + \frac{C_{F\alpha_s}(\mu_i)}{4\pi} G_2(\Delta_s, \hat{\omega}) \right] \\ + e^{V_H(m_b, \mu_i)} \int_0^{\Delta_s} d\hat{\omega} \hat{S}(\hat{\omega}, \mu_i) \frac{C_{F\alpha_s}(\mu_i)}{4\pi} G_3(\Delta_s, \hat{\omega}), \quad (100)$$

where

$$G_1(z) = T(a, z) \left\{ 1 + \frac{C_{F\alpha_s}(m_b)}{4\pi} H(a, z) + \frac{C_{F\alpha_s}(\mu_i)}{4\pi} [7 - \pi^2 - 3f_2(a, z) + 2f_3(a, z)] \right\} \quad (101)$$

contains the same functions T , H and f_n as defined in (94) and (95), but with all master integrals replaced by $I_n(b, 1) \rightarrow I_n(b, z)$. In addition, we need

$$G_2(\Delta_s, \hat{\omega}) = \int_0^{\mu_i^2/m_b} \frac{dP}{P} \left\{ \ln \frac{m_b P}{\mu_i^2} \left[k_1\left(\frac{\Delta_s}{P + \hat{\omega}}\right) - k_1\left(\frac{\Delta_s}{\hat{\omega}}\right) \right] + \left[k_2\left(\frac{\Delta_s}{P + \hat{\omega}}\right) - k_2\left(\frac{\Delta_s}{\hat{\omega}}\right) \right] \right\} \\ + \int_{\mu_i^2/m_b}^{\sqrt{s_0} - \hat{\omega}} \frac{dP}{P} \left[\ln \frac{m_b P}{\mu_i^2} k_1\left(\frac{\Delta_s}{P + \hat{\omega}}\right) + k_2\left(\frac{\Delta_s}{P + \hat{\omega}}\right) \right], \quad (102)$$

$$G_3(\Delta_s, \hat{\omega}) = \int_{\Delta_s}^{\sqrt{s_0}} \frac{dP}{P - \hat{\omega}} \left[\ln \frac{m_b(P - \hat{\omega})}{\mu_i^2} k_1\left(\frac{\Delta_s}{P}\right) + k_2\left(\frac{\Delta_s}{P}\right) \right],$$

where

$$k_1(z) = 4 \left[6I_1(2 - a, z) - 4I_1(3 - a, z) \right] = 4T(a, z), \quad (103) \\ k_2(z) = 4 \left[6I_2(2 - a, z) - 4I_2(3 - a, z) \right] - 3 \left[6I_1(2 - a, z) - 4I_1(3 - a, z) \right].$$

As mentioned above, the phase-space region near the cusp where $\hat{\omega} \sim \sqrt{s_0}$ or $P \sim \sqrt{s_0}$ gives a power-suppressed contribution to the decay rate. Using the explicit results for the functions G_i together with the asymptotic form of the shape function in (77), we find that the corresponding term is

$$F_M(s_0) \ni e^{V_H(m_b, \mu_i)} \frac{C_{F\alpha_s}(\mu_i)}{\pi} \frac{6}{(3 - a)^2} \left(\frac{\Delta_s}{\sqrt{s_0}} \right)^{3-a} \left(\frac{7}{4} + \frac{3}{3 - a} \right) + \dots, \quad (104)$$

where the dots represent higher-order power corrections. Whereas the fraction $F_M(s_0)$ is of $O(1)$ in power counting, the result (104) scales like $(\Lambda_{\text{QCD}}/m_b)^{(3-a)/2}$ for $s_0 \sim m_b \Lambda_{\text{QCD}}$. In the derivation of the formula for the event fraction we have neglected other power-suppressed terms with the same scaling. For consistency, we should therefore omit the term in (104), which can be done by replacing all occurrences of $\sqrt{s_0}$ in upper integration limits in (100) and (102) with ∞ . Only in that way we ensure that our calculations provide the unique leading-power contribution in the heavy-quark limit. We will use this prescription in our numerical analysis in Section 9.

Because of the presence of power corrections from a region in phase space where the collinear expansion breaks down, it is not clear to us how one would construct a systematic heavy-quark expansion for the fraction $F_M(s_0)$ beyond the leading order. Clarification of this point deserves further study.

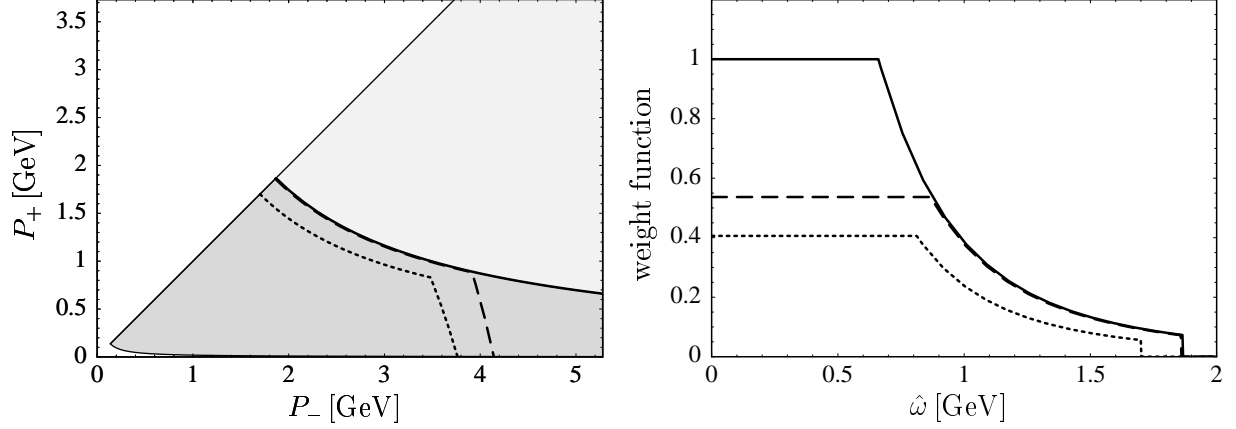


Figure 4: Phase-space constraints (left) and weight functions (right) for combined cuts on the hadronic and leptonic invariant mass: $(s_0, q_0^2) = (M_D^2, 0)$ (solid), $(M_D^2, 6 \text{ GeV}^2)$ (dashed), and $((1.7 \text{ GeV})^2, 8 \text{ GeV}^2)$ (dotted).

7.4 Combined cuts on hadronic and leptonic invariant mass

Bauer et al. have proposed to reduce the sensitivity to shape-function effects in the extraction of $|V_{ub}|$ by combining a cut on hadronic invariant mass with a cut $q^2 \geq q_0^2$ on the invariant mass squared of the lepton pair [46]. The first plot in Figure 4 shows that this eliminates a large portion of the events with large P_- . It is straightforward to study the effects of such a combined cut in the approximation where radiative corrections are neglected. For the corresponding event fraction at tree level, we obtain

$$F_{\text{comb}}(s_H \leq s_0, q^2 \geq q_0^2) = y_0^3 (2 - y_0) \int_0^{\Delta_s/y_0} d\hat{\omega} \hat{S}(\hat{\omega}) + \int_{\Delta_s/y_0}^{\sqrt{s_0}} d\hat{\omega} \hat{S}(\hat{\omega}) \left(\frac{\Delta_s}{\hat{\omega}} \right)^3 \left(2 - \frac{\Delta_s}{\hat{\omega}} \right), \quad (105)$$

where $y_0 = 1 - q_0^2/(m_b M_B)$, and $\Delta_s = s_0/M_B$ as above. For a fixed hadronic-mass cut s_0 , the effect of the cut on q^2 is to broaden the support of the first integral, while at the same time reducing its weight due to the prefactor. To illustrate this point, we show in the second plot in Figure 4 the weight functions under the integral with the shape function for three different choices of (s_0, q_0^2) . The sensitivity to the precise form of the shape function is reduced because the weight functions become progressively more shallow as the value of q_0^2 is raised. However, this reduction comes at the price of a significant reduction of the rate, raising questions about the validity of the assumption of quark-hadron duality. We will see in Section 9 that the *relative* uncertainty due to shape-function effects is not strongly reduced when imposing an additional cut on q^2 . We are therefore not convinced that it is worth paying this price.

7.5 Comparison with the literature

Before concluding this section, let us comment on results for inclusive B -decay spectra in the shape-function region previously published in the literature. Detailed predictions for

$\bar{B} \rightarrow X_u l^- \bar{\nu}$ decay distributions including shape-function effects were presented in [47] and [18]. In these papers, $O(\alpha_s)$ corrections were included at the level of the underlying parton spectra. In the last reference fully differential distributions are presented, which can be used to calculate arbitrary spectra and implement experimental cuts. Dedicated studies of the hadronic invariant mass spectrum can also be found in [48, 49, 50]. Similar analyses for the photon energy spectrum in $\bar{B} \rightarrow X_s \gamma$ decays were presented in [33, 51, 52]. In all these works, shape-function effects are implemented by convolving parton-model distributions with a primordial structure function, typically by replacing the b -quark mass in expressions for the parton spectra by a new variable $m_b^* = m_b + \omega$ [3]. This procedure is correct at tree level. However, it is no longer fully consistent when radiative corrections are included, because part of the $O(\alpha_s)$ corrections in the expressions for parton-level spectra are absorbed into the renormalization of the shape function. In particular, this changes the sign of the leading Sudakov logarithm, as can be seen by comparing the coefficients of the $\ln p^2/p^2$ terms in (18) and (26). This point has also been emphasized in [14]. An attempt to include radiative corrections to the spectra in a systematic way was made in [53], where in particular the evolution of the shape function has been addressed. Since our evolution equation does not agree with the one found by this author [31], our results for decay spectra are also in disagreement.

In [14], an expression has been presented for the double differential rate in the variables E_l and E_H , which (apart from a typo) is consistent with our findings. However, in this paper no distinction between $\alpha_s(m_b)$ and $\alpha_s(\mu_i)$ has been made in the next-to-leading order corrections, which entails significant perturbative uncertainties. Also, the important question of a physical definition of the b -quark mass has not been addressed. Whereas in our case all quantities are defined in a physical subtraction scheme and no reference to the b -quark mass is left in the final expressions for decay distributions (except as arguments of running couplings), the results of [14] contain explicit reference to the b -quark pole mass.

8 Model-independent relations between spectra

The decay spectra and event fractions discussed in the previous section are given in terms of weighted integrals of perturbative expressions with a non-perturbative shape function, which encodes hadronic physics related to the bound-state properties of the B meson. To use these formulae, one must take recourse to a model for the shape function, or (better) extract the shape function from a fit to experimental data. Alternatively, it is possible to derive model-independent relations between different decay distributions in which the shape function has been eliminated [1]. This makes use of the fact that at leading power in Λ_{QCD}/m_b shape-function effects in inclusive decays to light hadronic final states are described by a single universal (i.e., process independent) function. The most promising strategy is to relate event fractions in semileptonic $\bar{B} \rightarrow X_u l^- \bar{\nu}$ decays to a weighted integral over the $\bar{B} \rightarrow X_s \gamma$ photon spectrum, which at present provides the most direct access to the shape function.

While it is straightforward to derive such relations at tree level, radiative corrections introduce non-trivial complications [11, 12, 13]. In the following, we illustrate with a concrete example how such shape-function independent relations can be derived systematically within our framework. Since our formalism has yet to be applied to the $\bar{B} \rightarrow X_s \gamma$ photon spectrum,

we will instead derive a relation between the charged-lepton energy spectrum and a weighted integral over the P_+ spectrum in $\bar{B} \rightarrow X_u l^- \bar{\nu}$ decays. This relation serves as a prototype for all other shape-function independent relations between partially integrated decay rates. Note that the properties of the P_+ distribution are very similar to those of the $\bar{B} \rightarrow X_s \gamma$ photon spectrum in the sense that, at tree level, both spectra are directly given in terms of the shape function, e.g. $(1/\Gamma_{\text{tot}}) d\Gamma/dP_+ = \hat{S}(P_+) + \dots$. This connection, and its potential usefulness for an extraction of $|V_{ub}|$, has been noted earlier in [26].

Specifically, we wish to construct a *perturbative* weight function $w(\Delta, P_+)$ such that at leading power in Λ_{QCD}/m_b

$$\int_{E_0}^{M_B/2} dE_l \frac{d\Gamma}{dE_l} = \int_0^\Delta dP_+ w(\Delta, P_+) \frac{d\Gamma}{dP_+}, \quad \Delta = M_B - 2E_0. \quad (106)$$

This relation is independent of the shape function and hence insensitive to hadronic physics. The construction of the weight function is straightforward order by order in perturbation theory. Using the results of the previous section, we find

$$w(\Delta, P_+) = \frac{2(\Delta - P_+)}{M_B - P_+} \frac{3(4 - a)}{(6 - a)(2 - a)} \left\{ 1 + \frac{C_F \alpha_s(m_b)}{4\pi} h_1(a) + \frac{C_F \alpha_s(\mu_i)}{4\pi} \left[h_2(a) \ln \frac{m_b(\Delta - P_+)}{\mu_i^2} + h_3(a) \right] \right\}, \quad (107)$$

where

$$\begin{aligned} h_1(a) &= 2 - 2 \frac{3952 - 5416a + 2988a^2 - 838a^3 + 120a^4 - 7a^5}{(6 - a)(4 - a)^2(3 - a)(2 - a)^2} + c \frac{20 - 8a + a^2}{(6 - a)(4 - a)(2 - a)}, \\ h_2(a) &= -4 \frac{20 - 8a + a^2}{(6 - a)(4 - a)(2 - a)}, \\ h_3(a) &= \frac{5056 - 6744a + 3556a^2 - 942a^3 + 127a^4 - 7a^5}{(6 - a)(4 - a)^2(3 - a)(2 - a)^2}. \end{aligned} \quad (108)$$

Large logarithms of the form $[\alpha_s \ln(m_b/\mu_i)]^n$ and $\alpha_s[\alpha_s \ln(m_b/\mu_i)]^n$ are resummed exactly at next-to-leading order in renormalization-group improved perturbation theory. They enter the coefficient functions through the parameters a and c defined in (79).

In the equations for decay rates and spectra presented in Section 7, the dependence of the perturbative coefficients on the intermediate matching scale μ_i cancels against the scale dependence of the renormalized shape function $\hat{S}(\hat{\omega}, \mu_i)$. In practice, it is difficult to trace this cancellation if a model for the shape function at a fixed scale is employed. On the contrary, in the present case the weight function is formally independent of the scale μ_i , because there is nothing to cancel a potential μ_i dependence in (106). This fact can also be shown explicitly using the formulae given above. Expanding the resummed result for the weight function to first order in α_s , we obtain the simple expression

$$w(\Delta, P_+)|_{1\text{-loop}} = \frac{2(\Delta - P_+)}{M_B - P_+} \left[1 + \frac{C_F \alpha_s}{4\pi} \left(-\frac{5}{3} \ln \frac{\Delta - P_+}{m_b} - \frac{17}{36} \right) \right], \quad (109)$$

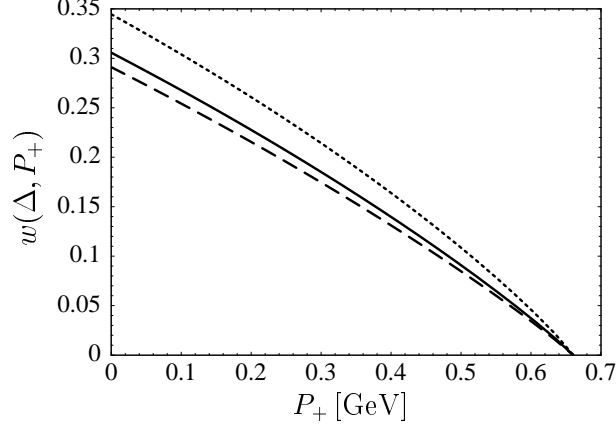


Figure 5: Weight function $w(\Delta, P_+)$ entering the rate relation (106) for $\Delta = M_D^2/M_B$ and three different choices of the intermediate scale, namely $\mu_i = 1.5$ GeV (solid), 2.0 GeV (dashed), and 1.0 GeV (dotted). The weight function is formally independent of μ_i .

in which the dependence on μ_i has canceled. However, since this formula contains a large logarithm and the scale to be used in α_s is undetermined, it should not be used for phenomenological applications.

Figure 5 shows results for the resummed weight function in the case where $\Delta = M_D^2/M_B \simeq 0.66$ GeV. The three curves refer to different values of the scale μ_i . The stability with respect to variations of the intermediate scale is very good except for the case of a very low scale ($\mu_i = 1$ GeV), for which the convergence of perturbation theory is expected to be poor.

The result (107) settles an old argument about the form of the weight function in relations such as (106). Leibovich et al. have presented a form for the weight function in a relation between the resummed $\bar{B} \rightarrow X_s \gamma$ and $\bar{B} \rightarrow X_u l^- \bar{\nu}$ decay rates, in which the kinematic variables corresponding to P_+ and Δ above enter in a most complicated form [11]. Their result has the unattractive feature that the integral over the weight function contains a Landau-pole singularity, which must be avoided by introducing a cutoff on the P_+ integral on the right-hand side of (106). A simpler form of the weight function, which is equivalent to (109) and contains only a single logarithm of the kinematic variables, has been promoted in [12]. Our exact result (107) obtained after renormalization-group improvement retains a simple form with only a single logarithm. Note, in particular, that our result does not exhibit any unphysical Landau singularities. We believe the resolution of the discrepancy has to do with the choice of the intermediate matching scale μ_i . Since the weight function is formally independent of μ_i , we are free to choose any value $\mu_i \sim \sqrt{m_b \Lambda_{\text{QCD}}}$. Taking the particular choice $\mu_i^2 = m_b(\Delta - P_+)$ would eliminate the logarithmic term in (107), however at the price of introducing a very complicated dependence on the kinematic variables Δ and P_+ via the dependence of the weight function on the quantity $a = \frac{16}{25} \ln[\alpha_s(\mu_i)/\alpha_s(m_b)]$. Also, with this choice the weight function would develop a Landau pole singularity at the point where the coupling $\alpha_s(\sqrt{m_b(\Delta - P_+)})$ gets strong, which happens for $(\Delta - P_+) \sim \Lambda_{\text{QCD}}^2/m_b$. All these unwanted features are avoided by using a fixed value for the intermediate scale, as we did in (107).

9 Numerical results

We are now ready to study the implications of our analysis for phenomenology. We start by deriving the numerical values for the shape-function mass and kinetic energy including errors. We then present a model for the shape function which satisfies all theoretical constraints, and study its behavior under renormalization-group evolution. Finally, we present numerical results for the various decay rates and spectra investigated in Section 7.

Throughout this paper we use the two-loop running coupling constant in the $\overline{\text{MS}}$ scheme, normalized such that $\alpha_s(M_Z) = 0.119$. We take $m_b = 4.65 \text{ GeV}$ as the default value for the b -quark mass in the shape-function scheme (see below), and $\mu_i = 1.5 \text{ GeV}$ as the standard choice of the intermediate matching scale. This corresponds to setting $\mu_i^2 = m_b \Lambda_{\text{had}}$ with a typical hadronic scale $\Lambda_{\text{had}} \approx 0.5 \text{ GeV}$. Note that this choice eliminates the appearance of the b -quark mass from the arguments of the logarithmic terms in the expressions for the decay rates. The values of the strong coupling evaluated at these scales are $\alpha_s(m_b) \simeq 0.222$ and $\alpha_s(\mu_i) \simeq 0.375$. The corresponding values of the perturbative parameters a and c defined in (79) are $a \simeq 0.335$ and $c \simeq 0.614$. Finally, the leading-order Sudakov factor in (78) takes the value $e^{V_H(m_b, \mu_i)} \simeq 1.21$.

9.1 Shape-function mass and kinetic energy

A value for the shape-function mass can be obtained by combining the relations (69) or (70) with existing predictions for the b -quark mass in the relevant renormalization schemes. The potential-subtracted mass at the scale $\mu_f = 2 \text{ GeV}$ has been determined from moments of the $b\bar{b}$ cross section and the mass of the $\Upsilon(1S)$ state [54]. Using the first relation in (70), the result of this paper implies $m_b^{\text{SF}}(2 \text{ GeV}, 2 \text{ GeV}) = m_b^{\text{PS}}(2 \text{ GeV}) = (4.59 \pm 0.08) \text{ GeV}$. From a similar analysis the kinetic mass has been determined at the scale $\mu_f = 2 \text{ GeV}$ to be $m_b^{\text{kin}}(1 \text{ GeV}) = (4.57 \pm 0.06) \text{ GeV}$ [41]. From the second relation in (70) it then follows that $m_b^{\text{SF}}(1 \text{ GeV}, 1 \text{ GeV}) = (4.65 \pm 0.06) \text{ GeV}$. Using relation (75) to compute the scale dependence of the shape-function mass, we obtain at the intermediate scale the values $m_b^{\text{SF}}(\mu_i, \mu_i) = (4.61 \pm 0.08) \text{ GeV}$ and $m_b^{\text{SF}}(\mu_i, \mu_i) = (4.65 \pm 0.06) \text{ GeV}$, respectively. Alternatively, we may use relation (69) in conjunction with an experimental determination of the b -quark pole mass from moments of inclusive $\bar{B} \rightarrow X_c l^- \bar{\nu}$ and $\bar{B} \rightarrow X_s \gamma$ decay spectra. Using the average value $\bar{\Lambda}_{\text{pole}} = (0.375 \pm 0.065) \text{ GeV}$ obtained from [55, 56, 57, 58], we find $m_b^{\text{SF}}(\mu_i, \mu_i) = (4.67 \pm 0.07) \text{ GeV}$. It is quite remarkable that these different determinations of the shape-function mass, which use rather different physics input, give highly consistent results. Combining them, we quote our default value for the shape-function mass at the intermediate scale $\mu_i = 1.5 \text{ GeV}$ as

$$m_b^{\text{SF}}(\mu_i, \mu_i) = (4.65 \pm 0.07) \text{ GeV}. \quad (110)$$

The corresponding $\bar{\Lambda}$ parameter is $\bar{\Lambda}(\mu_i, \mu_i) = (0.63 \pm 0.07) \text{ GeV}$.

A value of the kinetic-energy parameter in the shape-function scheme can be obtained from (71) or (72). Using the first relation combined with the experimental value $-\lambda_1 = (0.25 \pm 0.06) \text{ GeV}^2$ [56, 57, 58] yields $\mu_\pi^2(\mu_i, \mu_i) = (0.271 \pm 0.064) \text{ GeV}^2$. Alternatively, we may use the result for the kinetic-energy parameter obtained in the kinetic scheme, $[\mu_\pi^2(1 \text{ GeV})]_{\text{kin}} = (0.45 \pm 0.10) \text{ GeV}^2$ [41], to get from (72) the value $\mu_\pi^2(\mu_i, \mu_i) = (0.254 \pm 0.107) \text{ GeV}^2$. Again,

the two determinations are in very good agreement with each other. Combining them, we obtain

$$\mu_\pi^2(\mu_i, \mu_i) = (0.27 \pm 0.07) \text{ GeV}^2. \quad (111)$$

9.2 Model shape functions

In our analysis of decay rates below, we will adopt a model for the shape function $\hat{S}(\hat{\omega}, \mu_i)$ at the intermediate scale. We stress, however, that ultimately the shape function could be extracted from a fit to the photon spectrum in $\bar{B} \rightarrow X_s \gamma$ decays. This would largely reduce the theoretical uncertainties in our predictions.

For the purpose of illustration, we use a two-component ansatz for the shape function that is a generalization of the model employed in [18, 33]. The form we propose is

$$\hat{S}(\hat{\omega}, \mu) = \frac{N}{\Lambda} \left(\frac{\hat{\omega}}{\Lambda} \right)^{b-1} \exp \left(-b \frac{\hat{\omega}}{\Lambda} \right) - \frac{C_F \alpha_s(\mu)}{\pi} \frac{\theta(\hat{\omega} - \Lambda - \mu/\sqrt{e})}{\hat{\omega} - \Lambda} \left(2 \ln \frac{\hat{\omega} - \Lambda}{\mu} + 1 \right), \quad (112)$$

where Λ and b are model parameters, and Λ differs from the pole-scheme parameter $\bar{\Lambda}_{\text{pole}}$ by an amount of $O(\alpha_s(\mu))$. In the limit $\alpha_s(\mu) \rightarrow 0$ this function reduces to the one used in [18, 33]. The radiative tail ensures the correct leading asymptotic behavior of the shape function as displayed in (77). This in turn gives the correct power-like dependence of shape-function moments on the integration cutoff. In our model, this tail is glued onto a “primordial”, exponential function such that the combined result is continuous.

There are several non-trivial constraints on the parameters of the model. The normalization factor N is given by

$$N = \left[1 - \frac{C_F \alpha_s(\mu)}{\pi} \left(\frac{\pi^2}{24} - \frac{1}{4} \right) \right] \frac{b^b}{\Gamma(b)}, \quad (113)$$

which is determined such that the integral over the shape function from $\hat{\omega} = 0$ to $\mu_f + \bar{\Lambda}(\mu_f, \mu)$ coincides with the first expression in (74) up to second-order power corrections and exponentially small terms of order $e^{-\mu_f/\Lambda}$, which are negligible whenever μ_f is sufficiently large to trust our moment relations. By evaluating the first moment of the model shape function, we find that

$$\Lambda = \bar{\Lambda}_{\text{pole}} + \frac{C_F \alpha_s(\mu)}{\pi} \frac{2\mu}{\sqrt{e}} \quad (114)$$

to first order in α_s . From (69) it then follows that

$$\Lambda = \bar{\Lambda}(\mu_i, \mu_i) + \mu_i \left(\frac{2}{\sqrt{e}} - 1 \right) \frac{C_F \alpha_s(\mu_i)}{\pi} \simeq \bar{\Lambda}(\mu_i, \mu_i) + 51 \text{ MeV}. \quad (115)$$

Finally, the model parameter b can be adjusted to reproduce a given value for the second moment of the shape function.

Table 1 collects the parameters of the model shape functions at the intermediate scale $\mu_i = 1.5 \text{ GeV}$ corresponding to different values of $\bar{\Lambda}(\mu_i, \mu_i)$ and $\mu_\pi^2(\mu_i, \mu_i)$, as computed from the moment relations (74). These quantities are varied within their respective error ranges given in (110) and (111). Note that the Λ values in the table are in very good agreement with

Table 1: Parameters and moments of the model shape functions at the intermediate scale μ_i . The running quantities m_b^{SF} , $\bar{\Lambda}$, and μ_π^2 are defined in the shape-function scheme and evaluated at $\mu_f = \mu = \mu_i = 1.5 \text{ GeV}$.

Model	Lines	$m_b^{\text{SF}} [\text{GeV}]$	$\bar{\Lambda} [\text{GeV}]$	$\mu_\pi^2 [\text{GeV}^2]$	$\Lambda [\text{GeV}]$	b
S1	Dotted	4.72	0.56	0.20	0.611	2.84
S2				0.27	0.617	2.32
S3				0.34	0.626	1.92
S4	Solid	4.65	0.63	0.20	0.680	3.57
S5				0.27	0.685	2.93
S6				0.34	0.692	2.45
S7	Dashed	4.58	0.70	0.20	0.751	4.40
S8				0.27	0.753	3.61
S9				0.34	0.759	3.03

those obtained from the relation (115). The left-hand (right-hand) plot in Figure 6 shows three models for the shape function obtained by varying the parameters $\bar{\Lambda}$ and μ_π^2 in a correlated (anti-correlated) way. In both cases, the solid, dashed, and dotted curves refer to different values of $\bar{\Lambda}$, as indicated in the table.

In Figure 7 we illustrate how the shape function behaves under renormalization-group evolution. The sharply peaked solid line shows our model function evaluated with $\Lambda = 0.495 \text{ GeV}$ and $b = 3.0$, which we use as an ansatz for the function $\hat{S}(\hat{\omega}, \mu_0)$ at the low scale $\mu_0 = 1 \text{ GeV}$. For comparison, the dotted gray curve shows the default choice for the shape function adopted in [18, 33], which exhibits a very similar shape except for the missing radiative tail. The broad solid curve gives the shape function at the intermediate scale $\mu_i = 1.5 \text{ GeV}$ as obtained from the evolution equation (59). The barely visible dashed-dotted curve shows our default model for the function $\hat{S}(\hat{\omega}, \mu_i)$, which coincides with the solid line in the left-hand plot. The beautiful agreement of the two curves gives us confidence in the consistency of our models adopted for the shape function at the intermediate scale.

9.3 Predictions for decay spectra and event fractions

We are now ready to present our results for the decay spectra and partially integrated event fractions in $\bar{B} \rightarrow X_u l^- \bar{\nu}$ decays. In order to illustrate the sensitivity to shape-function effects we use the nine shape functions S1 through S9 in Table 1, thereby taking into account the full range of allowed values for the parameters $\bar{\Lambda}(\mu_i, \mu_i)$ and $\mu_\pi^2(\mu_i, \mu_i)$. For each physical quantity we draw three bands corresponding to the three different values of $\bar{\Lambda}$. The width of each band reflects the sensitivity to the variation of μ_π^2 . While one might in principle consider other functional forms for the shape function (which, however, must be consistent with the

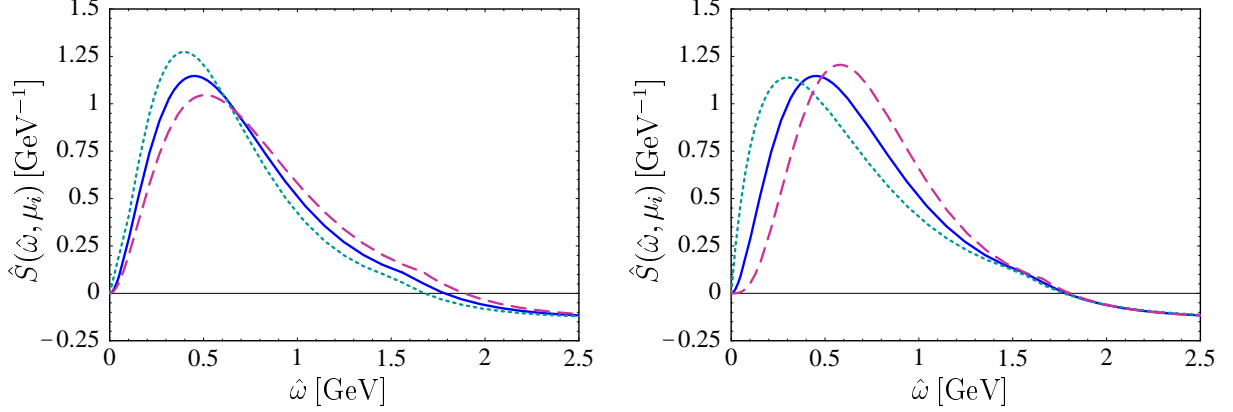


Figure 6: Various models for the shape function at the intermediate scale $\mu_i = 1.5 \text{ GeV}$, corresponding to different parameter settings in Table 1. Left: Functions S1, S5, S9 with “correlated” parameter variations. Right: Functions S3, S5, S7 with “anti-correlated” parameter variations.

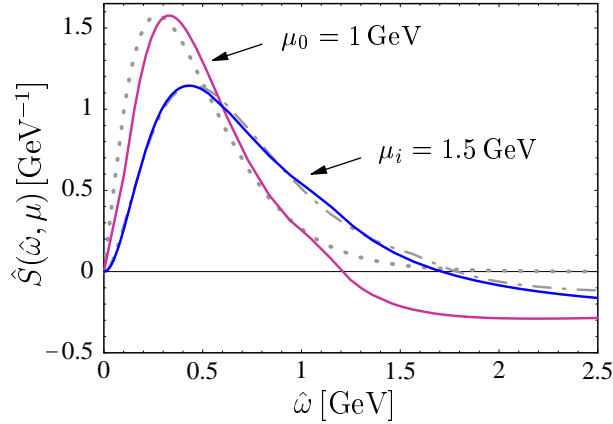


Figure 7: Renormalization-group evolution of a model shape function from a low scale μ_0 (sharply peaked solid curve) to the intermediate scale μ_i (broad solid curve). See the text for an explanation of the other curves.

asymptotic behavior as predicted by the operator product expansion), we believe that the variation of our results corresponding to the various models presents a realistic estimate of the shape-function sensitivity (see below).

The following predictions for spectra and rate fractions refer to the leading term in the heavy-quark expansion. Using our formalism, power corrections can be computed systematically to any order in Λ_{QCD}/m_b , by extending the two-step matching $\text{QCD} \rightarrow \text{SCET} \rightarrow \text{HQET}$ to the appropriate order. These power corrections fall into several categories, including corrections from phase space, kinematic factors, and subleading shape functions [59] (see [44, 60, 61] for tree-level discussions of these effects on various $\bar{B} \rightarrow X_u l^- \bar{\nu}$ spectra). Estimating the

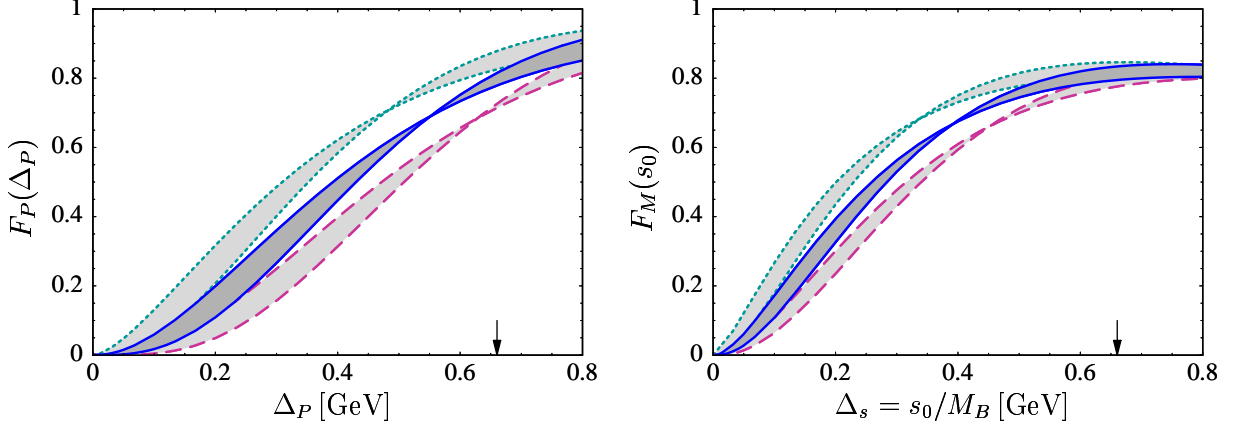


Figure 8: Fraction of $\bar{B} \rightarrow X_u l^- \bar{\nu}$ events with hadronic light-cone momentum $P_+ \leq \Delta_P$ (left), and fraction of events with hadronic invariant mass $s_H \leq s_0$ (right). In each plot, the three bands correspond to the values $\bar{\Lambda} = 0.63$ GeV (solid curves), 0.70 GeV (dashed curves), and 0.56 GeV (dotted curves). Their width reflects the sensitivity to the value of μ_π^2 varied in the range between 0.20 and 0.34 GeV². The arrow indicates the point at which the charm background starts.

corrections from phase space alone, we find that they typically change the leading-order predictions for partially integrated event fractions by about 10%. A more careful investigation of power corrections is left for future work. Finally, we note that our calculations would break down if the cuts on kinematic variables were taken to be too strict, because then the spectra would become dominated by hadronic resonance effects. Parametrically, this happens when the quantities Δ_P , Δ_s , or Δ_E become of order $\Lambda_{\text{QCD}}^2/M_B \sim 50$ MeV.

In Figure 8 we show predictions for the fractions of all $\bar{B} \rightarrow X_u l^- \bar{\nu}$ events with hadronic light-cone momentum $P_+ \leq \Delta_P$, and with hadronic invariant mass squared $s_H \leq s_0$. Recall that, for $\Delta_P = \Delta_s = s_0/M_B$, the hadronic invariant mass fraction F_M differs from the fraction F_P by the contribution of the events in the triangular region above the dashed line in Figure 3. Comparing the two plots, we observe that this additional contribution is predicted to be very small. (Note that for large values of Δ_s we even find a negative contribution to the rate from the triangle region for some choices of the shape function. This feature is unphysical and should be fixed by the inclusion of power corrections to our leading-order predictions.) The arrows on the horizontal axes indicate the points $\Delta_{P,s} = M_D^2/M_B$, beyond which final states containing charm hadrons are kinematically allowed. With this choice of the cut, both rate fractions capture about 80% of all events. While it is well known that a hadronic invariant mass cut $\sqrt{s_H} \leq M_D$ provides a very efficient discrimination against charm background [48, 49, 50], here we observe that the same is true for a cut on the P_+ variable. Cutting on P_+ offers the additional advantage of a “buffer zone” against charm background. Whereas the region in which charm final states are kinematically allowed borders the region with $\sqrt{s_H} \leq M_D$, it touches the phase-space region with $P_+ \leq M_D^2/M_B$ at only a single point (see Figure 3).

Our results for the charged-lepton energy spectrum $S_l(E_l) = (1/\Gamma_{\text{tot}}) (d\Gamma/dE_l)$, and for

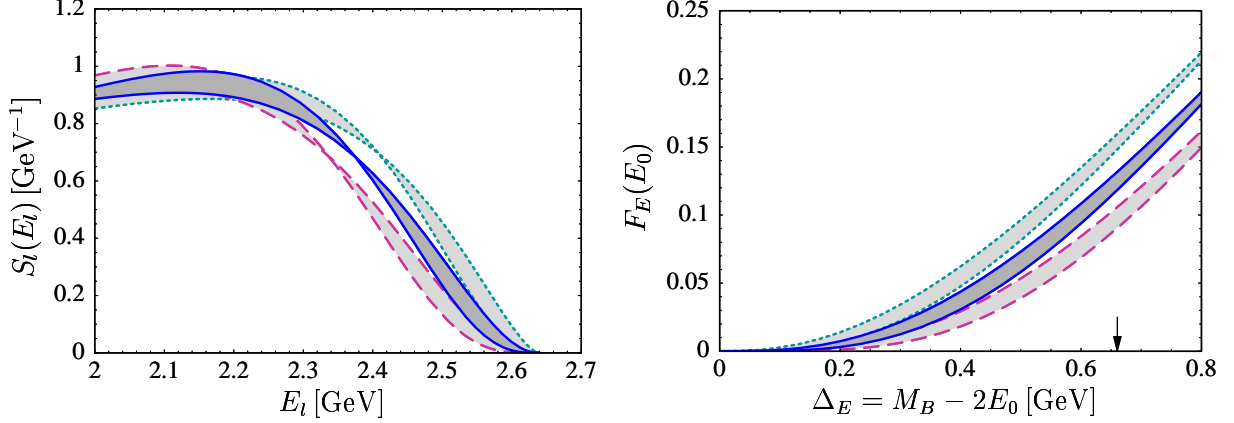


Figure 9: Charged-lepton energy spectrum in the region near the kinematic endpoint (left), and fraction of events with charged-lepton energy $E_l \geq E_0$ (right). The meaning of the bands and the arrow is the same as in Figure 8.

the event fraction with a cut $E_l \geq E_0$, are displayed in Figure 9. The right-hand plot shows that with $\Delta_E = M_D^2/M_B$ only about 10–15% of all events are retained, and the theoretical calculation is very sensitive to shape-function effects. Such a cut is therefore much less efficient than the cuts on hadronic invariant mass or P_+ . As a result, an extraction of $|V_{ub}|$ from the charged-lepton endpoint region is theoretically disfavored.

Let us now comment in more detail on the quantitative features of the results for the various event fractions. The most significant observation drawn from Figure 8 is that the shape-function sensitivity is rather small for values of Δ_P and Δ_s near the charm threshold. This is to some extent a consequence of our improved knowledge of the shape-function parameters. For instance, whereas in previous analyses the heavy-quark mass was varied in the range $m_b = (4.8 \pm 0.2)$ GeV [18], the mass defined in the shape-function scheme is known with much better accuracy, see (110). A similar statement applies to the width of the shape function and, more importantly, to its asymptotic behavior. Yet, the good convergence of the three bands in each plot seems puzzling at first sight, given that the model shape functions in Figure 6 are still rather different at $\hat{\omega} \approx 0.7$ GeV. The event fraction $F_P(\Delta_P)$, in particular, is *at tree level* given by the area under the shape-function curves between 0 and Δ_P . Remarkably, an interesting “focusing mechanism” arises beyond the tree approximation, which has its origin in a subtle interplay between the shape function and the jet function under the convolution integral in (93). The point is that the next-to-leading order corrections to the jet function (the terms proportional to $\alpha_s(\mu_i)$) contain a double-logarithmic singularity at the endpoint of the integration domain (at $\hat{\omega} = \Delta_P$), which comes with a *positive* coefficient. Consider now the integrals over the model shape functions from 0 to Δ_P , assuming that Δ_P is well beyond the maximum of the curves. The function with the smallest (largest) area takes the largest (smallest) value at the endpoint. When the shape functions are weighted with the jet function, the logarithmic spike at $\hat{\omega} = \Delta_P$ gives a contribution to the integral that is proportional to $\hat{S}(\Delta_P)$ and so is largest (smallest) for the function with the smallest (largest) area. The net result is to balance the differences in the areas and make the integrals converge more quickly

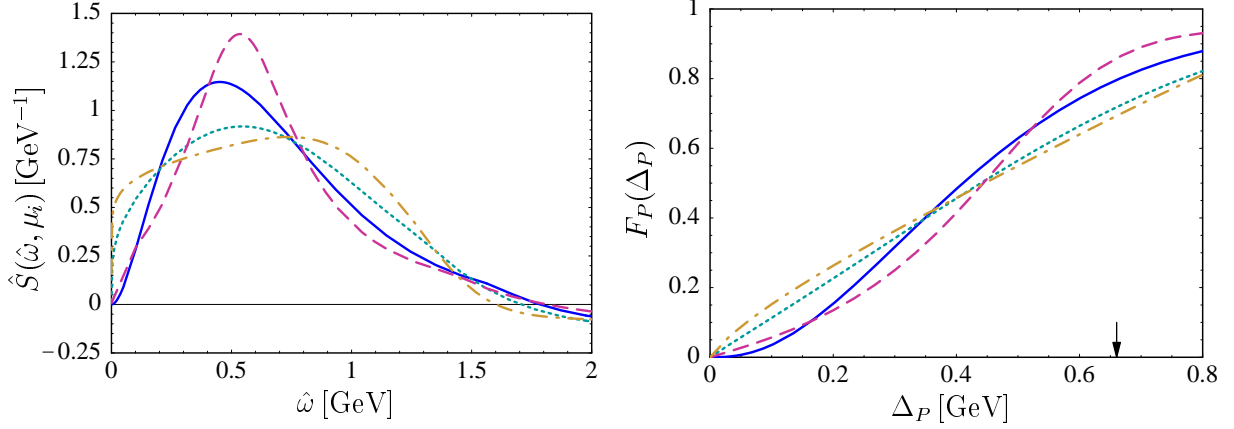


Figure 10: Left: Four examples of shape functions with identical normalization and first two moments, corresponding to $\bar{\Lambda}(\mu_i, \mu_i) = 0.63 \text{ GeV}$ and $\mu_\pi^2(\mu_i, \mu_i) = 0.27 \text{ GeV}^2$, but different functional form. Right: Corresponding results for the event fraction $F_P(\Delta_P)$.

toward a single value. The workings of this mechanism are nicely illustrated by comparing the results for the event fractions F_P and F_E in Figures 8 and 9. Whereas focusing takes place in the former case, the weight function under the integral for F_E in (92) vanishes at $\hat{\omega} = \Delta_E$, thereby suppressing the contribution from the logarithms in the jet function. This explains why no focusing is observed for the event fraction with a cut on charged-lepton energy.

Another way of thinking about this mechanism is to notice that the broadening of the shape function under renormalization-group evolution from a low scale up to the intermediate scale (right-hand plot in Figure 6) is a perturbative effect, which should not lead to an increased shape-function sensitivity. Because the convolution of the shape function with the jet and hard functions is independent of the scale μ_i , the broadening of the shape function must be compensated by perturbative logarithms in the jet function.

Note that it is crucial for this mechanism that the logarithmic terms in the jet function give a *positive* contribution near $\hat{\omega} = \Delta_P$. This focusing effect did not take place in earlier studies such as [18, 47, 48, 49, 50], where parton-model spectra were convoluted with a primordial shape function. As mentioned earlier, in the parton model the leading Sudakov logarithm comes with the opposite (negative) sign, hence causing an anti-focusing effect of the radiative corrections. This also explains why our prediction for the hadronic invariant mass fraction F_M exhibits a smaller shape-function sensitivity than what has been found in most previous analyses.

In addition to their dependence on the moment parameters $\bar{\Lambda}$ and μ_π^2 , our predictions are also sensitive to the functional form adopted for the shape function. In order to study this sensitivity we have constructed four shape functions with identical zeroth, first, and second moments, but rather different functional forms. They are shown in the left-hand plot in Figure 10. Some of these choices are intentionally rather extreme, given what is known about the shape function from the measurement of the $\bar{B} \rightarrow X_s \gamma$ photon spectrum [55]. The point is to illustrate that even drastic variations of the functional form do not invalidate the predictions

Table 2: Comparison of different theoretical methods using inclusive B -decay rates to extract the CKM matrix element $|V_{ub}|$. The error on the efficiency represents the sensitivity to the shape function only. All results refer to the leading term in the heavy-quark expansion.

Method	Cut	Efficiency
Hadronic invariant mass	$s_H \leq M_D^2$	$(81.4^{+3.2}_{-3.7})\%$
	$s_H \leq (1.7 \text{ GeV})^2$	$(78.2^{+4.9}_{-5.2})\%$
	$s_H \leq (1.55 \text{ GeV})^2$	$(72.7^{+6.4}_{-6.3})\%$
Hadronic P_+	$P_+ \leq \frac{M_D^2}{M_B} = 0.66 \text{ GeV}$	$(79.6^{+8.2}_{-8.2})\%$
	$P_+ \leq 0.55 \text{ GeV}$	$(69.0^{+9.7}_{-12.1})\%$
Charged-lepton energy	$E_l \geq \frac{M_B^2 - M_D^2}{2M_B} = 2.31 \text{ GeV}$	$(12.5^{+3.4}_{-3.5})\%$
	$E_l \geq 2.2 \text{ GeV}$	$(22.2^{+3.2}_{-3.6})\%$
Combined (s_H, q^2) cuts [tree level only]	$s_H \leq M_D^2, q^2 \geq 0$	$(74.6^{+5.1}_{-5.1})\%$
	$s_H \leq M_D^2, q^2 \geq 6 \text{ GeV}^2$	$(45.7^{+1.8}_{-2.0})\%$
	$s_H \leq (1.7 \text{ GeV})^2, q^2 \geq 8 \text{ GeV}^2$	$(33.4^{+1.6}_{-1.8})\%$

presented earlier in this section. The right-hand plot in Figure 10 shows, as an example, the results for the event fraction $F_P(\Delta_P)$ obtained using the four functions. Comparing this plot with the corresponding one in Figure 8 shows that at present the variation of the parameters $\bar{\Lambda}$ and μ_π^2 covers the uncertainty in the functional form. We have checked that this is also true for the other decay distributions studied here. However, if in the future the errors on $\bar{\Lambda}$ and μ_π^2 were reduced significantly, one should also include the sensitivity to the functional form in the error estimate.

A summary of our phenomenological results can be found in Table 2. For a variety of different experimental cuts we report the fractions of the contained $\bar{B} \rightarrow X_u l^- \bar{\nu}$ events and indicate how these fractions vary under the variation of the shape-function models. In all cases the goal is to reject the charm background as efficiently as possible, while preserving a sufficiently large fraction of the signal events so as to obtain a reliable determination of the CKM matrix element $|V_{ub}|$. We emphasize that our results refer to the leading term in the heavy-quark expansion, and that the rates are expected to be modified somewhat by power corrections. The uncertainties quoted on the contained event fractions reflect their sensitivity to shape-function effects only. No other theoretical uncertainties are included in these estimates.

The first portion of the table contains results for the event fractions with a cut on hadronic invariant mass. The first line corresponds to the “ideal” cut $\sqrt{s_H} \leq M_D$, which in theory eliminates the charm background entirely. This cut retains about 80% of all $\bar{B} \rightarrow X_u l^- \bar{\nu}$ events.

In practice, spill-over from final states containing charm hadrons in a realistic measurement requires to lower the cut on hadronic invariant mass to values slightly below M_D . Two typical choices are also covered in the table. Lowering the cut reduces the contained event fraction by modest amounts, while the sensitivity to shape-function effects increases markedly. Yet, even with a cut at 1.55 GeV the uncertainty on $|V_{ub}|$ would still amount to only 4%.

The second portion of the table shows two examples of cuts on the hadronic light-cone momentum P_+ . With the “ideal” cut $P_+ \leq M_D^2/M_B$ about 80% of all events are contained, which is as good as with the hadronic invariant mass cut. The sensitivity to shape-function effects is somewhat more pronounced but still at a very acceptable level. The corresponding uncertainty on $|V_{ub}|$ is about 5%. Since the P_+ spectrum is directly related to the photon energy spectrum in $\bar{B} \rightarrow X_s \gamma$ decays, this uncertainty can be reduced further by using experimental information on the photon spectrum. Due to the fact that there is a “buffer zone” separating the signal events from the charm background, we expect less spill-over than in the case of a cut on hadronic invariant mass. It may therefore be experimentally feasible to implement the cutoff near the optimal value. However, even if the value of Δ_P must be lowered by a small amount, the efficiency remains high and the shape function sensitivity at an acceptable level (see the second entry in the table).

The third portion of the table shows results for the case of a cut on the energy of the charged lepton. The efficiency is obviously much reduced in this case, even if the cut can be relaxed into the region where some charm background is present (second entry). The theoretical calculations are therefore more prone to uncertainties from other effects such as weak annihilation [62].

In the lower portion of the table we give results for some combined cuts on hadronic and leptonic invariant mass, which have been briefly discussed in Section 7.4. Contrary to the other cases, these numbers refer to the tree-level approximation and so should be taken with caution. For reference, we quote again the (tree-level) result for the pure hadronic invariant mass cut, which differs significantly from the corresponding result including radiative corrections. While the additional cut on leptonic q^2 reduces the shape-function sensitivity, it comes along with a strong reduction of the efficiency. For instance, the combined cut $\sqrt{s_H} \leq 1.7$ GeV and $q^2 \geq 8$ GeV² employed in a recent analysis of the Belle Collaboration [63] has an efficiency of about 33% (at tree level and leading order in Λ_{QCD}/m_b), which is much smaller than the efficiency of the pure hadronic invariant mass cut $\sqrt{s_H} \leq 1.7$ GeV. However, the sensitivity to shape-function effects is only slightly better in the case of the combined cut.

As a final remark, let us comment on the applicability of the theoretical framework developed in this work. According to Figure 3 most of the $\bar{B} \rightarrow X_u l^- \bar{\nu}$ events are located in the shape-function region of large P_- and small to moderate P_+ . Our approach is based on a systematic heavy-quark expansion valid in that region of phase space. It allows us to calculate inclusive decay rates integrated over domains $\Delta P_- \sim M_B$ and $\Delta P_+ \ll M_B$, where typically $\Delta P_+ \sim \Lambda_{\text{QCD}}$. (In the examples above, $\Delta P_+ = \Delta_E$, Δ_P , or Δ_s , respectively.) While the corresponding predictions for decay spectra and event fractions are sufficient to analyse experimental data over most of the phase space relevant to measurements of the CKM matrix element $|V_{ub}|$, it would be of interest to extend the validity of the theoretical description outside the shape-function region. In the case where $\Delta P_- \sim \Delta P_+ \sim M_B$ are both large, the decay spectra can be computed using a local operator product expansion. An interesting question is

whether it will be possible to match these two approaches in some intermediate region of ΔP_+ values that are numerically (but not parametrically) large compared with Λ_{QCD} . If the two predictions were to agree in an overlap region, this could be used to construct a theoretical description of inclusive $\bar{B} \rightarrow X_u l^- \bar{\nu}$ decay distributions that is valid over the entire phase space. While this is an exciting prospect, we note that performing a systematic operator product expansion in the overlap region is far from trivial. Because of the hierarchy of scales $\Delta P_+^2 \ll \Delta P_+ M_B \ll M_B^2$, again a two-step procedure is in order. An example of such an approach can be found in [64].

10 Conclusions

We have calculated differential spectra and partially integrated event fractions for the inclusive semileptonic decays $\bar{B} \rightarrow X_u l^- \bar{\nu}$ at next-to-leading order in renormalization-group improved perturbation theory, and at leading power in the heavy-quark expansion. The hadronic tensor entering the differential decay rates has been factorized into perturbatively calculable hard and jet functions, H_{ij} and J , which we give to one-loop order, and a universal shape function S containing non-perturbative physics below an intermediate scale $\mu_i \sim \sqrt{m_b \Lambda_{\text{QCD}}}$. This factorization has been obtained by matching QCD onto soft-collinear effective theory to integrate out hard fluctuations of order m_b , and by matching the result further onto heavy-quark effective theory (HQET) to integrate out hard-collinear modes at the intermediate mass scale. Large logarithms have been resummed by solving the renormalization-group equation for the hard kernels, evolving the functions H_{ij} from the hard scale $\mu_h \sim m_b$ down to the intermediate scale μ_i . In order to make use of the resulting expression for the hadronic tensor, the shape function is needed at this intermediate scale μ_i . We have derived the anomalous dimension of the shape function at one-loop order and given an exact analytic solution of the resulting renormalization-group equation. Our solution can be applied to any model for the shape function obtained at any scale. Alternatively, if the shape function is treated as a phenomenological quantity, renormalizing it at the scale μ_i avoids doing perturbation theory at a low hadronic scale.

Moments of the shape function are often identified with HQET parameters such as $\bar{\Lambda}$ and λ_1 . This identification was so far only understood at tree level. We have discovered the appearance of a radiative tail of the shape function that vanishes slower than $1/|\omega|$. This feature renders all shape-function moments (including the normalization integral) ultra-violet divergent. To define the moments consistently we have introduced a hard ultra-violet cutoff Λ_{UV} on the integrals over ω . This is natural, since in any physical process the shape function will only be integrated over a finite interval. The dependence of the moments on this cutoff can be controlled using a local operator product expansion, which has enabled us to derive reliable perturbative relations between shape-function moments and HQET parameters. We have also obtained a formula for the normalization integral over the shape function as a function of Λ_{UV} , and from it a model-independent prediction for the asymptotic behavior of the shape function for large values of $|\omega|$. Surprisingly, this analysis reveals that the shape function has a negative tail and so is not positive definite, contrary to common expectation.

Due to the fact that the b -quark pole mass, and with it the HQET parameter $\bar{\Lambda}$, suffers

from infra-red renormalon ambiguities, it is favorable to replace m_b^{pole} by a short-distance mass defined in a physical subtraction scheme. We have argued that the most natural definition for applications to inclusive spectra is to define a “shape-function mass” $m_b^{\text{SF}}(\Lambda_{\text{UV}}, \mu)$ by enforcing that the first moment of the renormalized shape function vanish for any given value of the cutoff Λ_{UV} . The dependence of the shape-function mass on the cutoff Λ_{UV} and on the dimensional regularization scale μ is controlled by evolution equations, which can be trusted as long as both scales are much larger than Λ_{QCD} . Using a similar approach, we have defined a running kinetic-energy parameter $\mu_\pi^2(\Lambda_{\text{UV}}, \mu)$ in the shape-function scheme, which can be used to replace the (ambiguous) HQET parameter λ_1 . We relate our new parameters to some previous, physical definitions of m_b and μ_π^2 . All of these new insights restrict model building of the shape function drastically. We give expressions for some model shape functions that are fully consistent with all constraints, albeit leaving enough freedom to accommodate future experimental constraints from the $\bar{B} \rightarrow X_s \gamma$ photon spectrum.

In the second part of the paper we have applied our results to make predictions for several interesting $\bar{B} \rightarrow X_u l^- \bar{\nu}$ decay distributions and spectra in the shape-function region of large hadronic energy ($E_H \sim M_B$) and small hadronic invariant mass ($s_H \sim M_B \Lambda_{\text{QCD}}$). We have presented results for event fractions with cuts on the charged-lepton energy, hadronic invariant mass, or hadronic light-cone momentum $P_+ = E_H - |\vec{P}_H|$, where in each case the cuts are chosen so as to reject background from $\bar{B} \rightarrow X_c l^- \bar{\nu}$ decays. These formulae are presented as convolution integrals of weight functions with the shape function renormalized at the intermediate scale μ_i . Our results are valid at next-to-leading order in renormalization-group improved perturbation theory and at leading power in the heavy-quark expansion. The discussion of these distributions is most transparent in terms of the hadronic phase space for the two variables $P_\pm = E_H \mp |\vec{P}_H|$, which we have studied in some detail (see Figure 3).

An important outcome of our phenomenological analysis is the finding that a cut $P_+ \leq M_D^2/M_B \simeq 0.66 \text{ GeV}$ on the hadronic light-cone momentum eliminates the charm background while containing the vast majority of all $\bar{B} \rightarrow X_u l^- \bar{\nu}$ events. At leading power in Λ_{QCD}/m_b this cut has an efficiency of about 80%, which is almost as efficient as the cut $\sqrt{s_H} \leq M_D$ on hadronic invariant mass. A cut on P_+ offers several advantages over a cut on hadronic invariant mass. First, it provides a “buffer zone” against charm background, which borders the signal region at only a single point in phase space. Secondly, the hadronic physics affecting the P_+ spectrum is directly related to the hadronic physics affecting the $\bar{B} \rightarrow X_s \gamma$ photon energy spectrum (the two spectra are identical at tree level). This implies that a simple, shape-function independent relation between the two distributions can be derived, which could be used to eliminate hadronic uncertainties (at least at leading power in Λ_{QCD}/m_b). Finally, as we have pointed out, the calculation of the hadronic invariant mass distribution suffers from the fact that it includes a region in phase space where the collinear expansion breaks down. While this region gives only a power-suppressed contribution to the rate, its presence might cause complications if the calculation is taken beyond the leading power. The P_+ spectrum, on the other hand, can be accurately calculated beyond the leading order using the methods developed here. It would be a most useful quantity to measure.

Using our formalism, shape-function independent relations between different decay distributions can be derived in a systematic way, and they are free of unphysical Landau singularities. As an example, we have derived a relation between the charged-lepton energy spectrum

and a weighted integral over the P_+ spectrum in $\bar{B} \rightarrow X_u l^- \bar{\nu}$ decays. This formula serves as a prototype for other relations, including the more useful relation between the P_+ spectrum and the photon energy spectrum in $\bar{B} \rightarrow X_s \gamma$ decays, which can be used for a new, high-precision determination of $|V_{ub}|$ once the technology developed in this paper has been applied to $\bar{B} \rightarrow X_s \gamma$ decays.

Finally, let us reiterate that the results presented here are valid at leading power in Λ_{QCD}/m_b . While it may be laborious to calculate the next term in the expansion, this can be systematically done in our formalism (with the possible exception of the hadronic invariant mass spectrum), and we believe it must be done in order to achieve a theoretical accuracy in the prediction of decay spectra at the 10% level. If this level of precision can be achieved, it would for the first time lead the way toward a precision measurement of the CKM matrix element $|V_{ub}|$ with a theoretical error at the 5% level. This would be worth the effort.

Note added: After this work was completed, we became aware of a paper by Grozin and Korchemsky [65], where the evolution kernel for the shape function in (45) was calculated at two-loop order. Our one-loop results in (46) agree with their findings.

Acknowledgments: This research was supported by the National Science Foundation under Grant PHY-0098631.

References

- [1] M. Neubert, Phys. Rev. D **49**, 3392 (1994) [hep-ph/9311325]; Phys. Rev. D **49**, 4623 (1994) [hep-ph/9312311].
- [2] I. I. Y. Bigi, M. A. Shifman, N. G. Uraltsev and A. I. Vainshtein, Int. J. Mod. Phys. A **9**, 2467 (1994) [hep-ph/9312359].
- [3] T. Mannel and M. Neubert, Phys. Rev. D **50**, 2037 (1994) [hep-ph/9402288].
- [4] J. Chay, H. Georgi and B. Grinstein, Phys. Lett. B **247**, 399 (1990).
- [5] I. I. Y. Bigi, N. G. Uraltsev and A. I. Vainshtein, Phys. Lett. B **293**, 430 (1992) [Erratum-ibid. B **297**, 477 (1993)] [hep-ph/9207214]; I. I. Y. Bigi, M. A. Shifman, N. G. Uraltsev and A. I. Vainshtein, Phys. Rev. Lett. **71**, 496 (1993) [hep-ph/9304225]; B. Blok, L. Koyrakh, M. A. Shifman and A. I. Vainshtein, Phys. Rev. D **49**, 3356 (1994) [Erratum-ibid. D **50**, 3572 (1994)] [hep-ph/9307247].
- [6] A. V. Manohar and M. B. Wise, Phys. Rev. D **49**, 1310 (1994) [hep-ph/9308246].
- [7] A. F. Falk, E. Jenkins, A. V. Manohar and M. B. Wise, Phys. Rev. D **49**, 4553 (1994) [hep-ph/9312306].
- [8] G. P. Korchemsky and G. Sterman, Phys. Lett. B **340**, 96 (1994) [hep-ph/9407344].
- [9] R. Akhouri and I. Z. Rothstein, Phys. Rev. D **54**, 2349 (1996) [hep-ph/9512303].

- [10] C. W. Bauer, S. Fleming and M. E. Luke, Phys. Rev. D **63**, 014006 (2001) [hep-ph/0005275].
- [11] A. K. Leibovich, I. Low and I. Z. Rothstein, Phys. Rev. D **61**, 053006 (2000) [hep-ph/9909404].
- [12] M. Neubert, Phys. Lett. B **513**, 88 (2001) [hep-ph/0104280].
- [13] A. K. Leibovich, I. Low and I. Z. Rothstein, Phys. Lett. B **513**, 83 (2001) [hep-ph/0105066].
- [14] C. W. Bauer and A. V. Manohar, hep-ph/0312109.
- [15] B. O. Lange and M. Neubert, Phys. Rev. Lett. **91**, 102001 (2003) [hep-ph/0303082].
- [16] C. Balzereit, T. Mannel and W. Kilian, Phys. Rev. D **58**, 114029 (1998) [hep-ph/9805297].
- [17] For a review, see: M. Neubert, Phys. Rept. **245**, 259 (1994) [hep-ph/9306320].
- [18] F. De Fazio and M. Neubert, JHEP **9906**, 017 (1999) [hep-ph/9905351].
- [19] C. W. Bauer, S. Fleming, D. Pirjol and I. W. Stewart, Phys. Rev. D **63**, 114020 (2001) [hep-ph/0011336].
- [20] C. W. Bauer, D. Pirjol and I. W. Stewart, Phys. Rev. D **65**, 054022 (2002) [hep-ph/0109045].
- [21] J. Chay and C. Kim, Phys. Rev. D **65**, 114016 (2002) [hep-ph/0201197].
- [22] M. Beneke, A. P. Chapovsky, M. Diehl and T. Feldmann, Nucl. Phys. B **643**, 431 (2002) [hep-ph/0206152].
- [23] R. J. Hill and M. Neubert, Nucl. Phys. B **657**, 229 (2003) [hep-ph/0211018].
- [24] M. Beneke and T. Feldmann, Phys. Lett. B **553**, 267 (2003) [hep-ph/0211358].
- [25] T. Becher, R. J. Hill and M. Neubert, Phys. Rev. D **69**, 054017 (2004) [hep-ph/0308122].
- [26] T. Mannel and S. Recksiegel, Phys. Rev. D **60**, 114040 (1999) [hep-ph/9904475].
- [27] U. Aglietti, M. Ciuchini and P. Gambino, Nucl. Phys. B **637**, 427 (2002) [hep-ph/0204140].
- [28] T. Mannel and S. Recksiegel, Phys. Rev. D **63**, 094011 (2001) [hep-ph/0009268].
- [29] S. W. Bosch, R. J. Hill, B. O. Lange and M. Neubert, Phys. Rev. D **67**, 094014 (2003) [hep-ph/0301123].
- [30] G. P. Korchemsky and A. V. Radyushkin, Nucl. Phys. B **283**, 342 (1987); I. A. Korchemskaya and G. P. Korchemsky, Phys. Lett. B **287**, 169 (1992).

- [31] U. Aglietti and G. Ricciardi, Phys. Lett. B **466**, 313 (1999) [hep-ph/9907501].
- [32] A. G. Grozin and M. Neubert, Phys. Rev. D **55**, 272 (1997) [hep-ph/9607366].
- [33] A. L. Kagan and M. Neubert, Eur. Phys. J. C **7**, 5 (1999) [hep-ph/9805303].
- [34] I. Bigi and N. Uraltsev, Int. J. Mod. Phys. A **17**, 4709 (2002) [hep-ph/0202175].
- [35] A. F. Falk, M. Neubert and M. E. Luke, Nucl. Phys. B **388**, 363 (1992) [hep-ph/9204229].
- [36] I. I. Y. Bigi, M. A. Shifman, N. G. Uraltsev and A. I. Vainshtein, Phys. Rev. D **50**, 2234 (1994) [hep-ph/9402360].
- [37] M. Beneke and V. M. Braun, Nucl. Phys. B **426**, 301 (1994) [hep-ph/9402364].
- [38] I. I. Y. Bigi, M. A. Shifman, N. Uraltsev and A. I. Vainshtein, Phys. Rev. D **56**, 4017 (1997) [hep-ph/9704245].
- [39] M. Beneke, Phys. Lett. B **434**, 115 (1998) [hep-ph/9804241].
- [40] I. I. Y. Bigi, M. A. Shifman and N. Uraltsev, Ann. Rev. Nucl. Part. Sci. **47**, 591 (1997) [hep-ph/9703290].
- [41] D. Benson, I. I. Bigi, T. Mannel and N. Uraltsev, Nucl. Phys. B **665**, 367 (2003) [hep-ph/0302262].
- [42] G. Martinelli, M. Neubert and C. T. Sachrajda, Nucl. Phys. B **461**, 238 (1996) [hep-ph/9504217]; M. Neubert, Phys. Lett. B **393**, 110 (1997) [hep-ph/9610471].
- [43] For a recent discussion, see: I. I. Y. Bigi and N. Uraltsev, Int. J. Mod. Phys. A **16**, 5201 (2001) [hep-ph/0106346].
- [44] C. W. Bauer, M. Luke and T. Mannel, Phys. Lett. B **543**, 261 (2002) [hep-ph/0205150].
- [45] M. Neubert, Phys. Lett. B **543**, 269 (2002) [hep-ph/0207002].
- [46] C. W. Bauer, Z. Ligeti and M. E. Luke, Phys. Rev. D **64**, 113004 (2001) [hep-ph/0107074].
- [47] R. D. Dikeman and N. G. Uraltsev, Nucl. Phys. B **509**, 378 (1998) [hep-ph/9703437].
- [48] I. I. Y. Bigi, R. D. Dikeman and N. Uraltsev, Eur. Phys. J. C **4**, 453 (1998) [hep-ph/9706520].
- [49] A. F. Falk, Z. Ligeti and M. B. Wise, Phys. Lett. B **406**, 225 (1997) [hep-ph/9705235].
- [50] M. Jezabek, T. Mannel, B. Postler and P. Urban, Phys. Lett. B **512**, 65 (2001) [hep-ph/0101330].
- [51] R. D. Dikeman, M. A. Shifman and N. G. Uraltsev, Int. J. Mod. Phys. A **11**, 571 (1996) [hep-ph/9505397].

- [52] A. K. Leibovich and I. Z. Rothstein, Phys. Rev. D **61**, 074006 (2000) [hep-ph/9907391].
- [53] U. Aglietti, Nucl. Phys. B **610**, 293 (2001) [hep-ph/0104020].
- [54] M. Beneke and A. Signer, Phys. Lett. B **471**, 233 (1999) [hep-ph/9906475].
- [55] S. Chen *et al.* [CLEO Collaboration], Phys. Rev. Lett. **87**, 251807 (2001) [hep-ex/0108032].
- [56] D. Cronin-Hennessy *et al.* [CLEO Collaboration], Phys. Rev. Lett. **87**, 251808 (2001) [hep-ex/0108033].
- [57] A. H. Mahmood *et al.* [CLEO Collaboration], Phys. Rev. D **67**, 072001 (2003) [hep-ex/0212051].
- [58] B. Aubert *et al.* [BaBar Collaboration], hep-ex/0307046.
- [59] C. W. Bauer, M. E. Luke and T. Mannel, Phys. Rev. D **68**, 094001 (2003) [hep-ph/0102089].
- [60] A. K. Leibovich, Z. Ligeti and M. B. Wise, Phys. Lett. B **539**, 242 (2002) [hep-ph/0205148].
- [61] C. N. Burrell, M. E. Luke and A. R. Williamson, Phys. Rev. D **69**, 074015 (2004) [hep-ph/0312366].
- [62] M. B. Voloshin, Phys. Lett. B **515**, 74 (2001) [hep-ph/0106040].
- [63] H. Kakuno *et al.* [Belle Collaboration], Phys. Rev. Lett. **92**, 101801 (2004) [hep-ex/0311048].
- [64] T. Becher and M. Neubert, Phys. Lett. B **535**, 127 (2002) [hep-ph/0105217].
- [65] A. G. Grozin and G. P. Korchemsky, Phys. Rev. D **53**, 1378 (1996) [hep-ph/9411323].